# Distribution of individual wave overtopping volumes at rubble mound seawalls

Koosheh, Ali; Etemad-Shahidi, Amir; Cartwright, Nick; Tomlinson, Rodger; van Gent, Marcel R.A.

**DOI**
10.1016/j.coastaleng.2022.104173

**Publication date**
2022

**Document Version**
Final published version

**Published in**
Coastal Engineering

**Citation (APA)**
Koosheh, A., Etemad-Shahidi, A., Cartwright, N., Tomlinson, R., & van Gent, M. R. A. (2022). Distribution of individual wave overtopping volumes at rubble mound seawalls. *Coastal Engineering*, *177*, Article 104173. https://doi.org/10.1016/j.coastaleng.2022.104173

Coastal Engineering 177 (2022) 104173

Contents lists available at ScienceDirect

Coastal Engineering

journal homepage: www.elsevier.com/locate/coastaleng

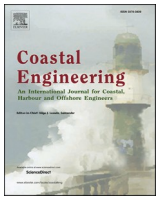

# Distribution of individual wave overtopping volumes at rubble mound seawalls

Ali Koosheh [a,*], Amir Etemad-Shahidi [a,b], Nick Cartwright [a], Rodger Tomlinson [c], Marcel R.A. van Gent [d,e]

[a] School of Engineering and Built Environment, Griffith University, Southport, QLD, 4222, Australia
[b] School of Engineering, Edith Cowan University, WA, 6027, Australia
[c] Coastal and Marine Research Centre, Griffith University, Southport, QLD, 4222, Australia
[d] Department of Coastal Structures & Waves, Deltares, 2600, MH, Delft, the Netherlands
[e] Department of Hydraulic Engineering, TU Delft, 2628, CN, Delft, the Netherlands

ARTICLE INFO

*Keywords:*
Individual wave overtopping volumes distribution
Rubble mound seawall
Probability of overtopping
Weibull distribution
Exponential distribution

ABSTRACT

For a safe design of a rubble mound seawall, overtopping characteristics such as the mean overtopping discharge ($q$) and the maximum individual overtopping volume ($V_{max}$) should be limited. Unlike $q$, the estimation of $V_{max}$ is more complex and requires a wave-by-wave analysis of overtopping as well as a statistical analysis. The present study contributes to the knowledge of the distribution of individual overtopping volumes and the estimation of $V_{max}$ at rubble mound seawalls. A total of 135, small-scale 2D physical model tests were conducted across a practical range of crest freeboards and considered the slopes of 1:1.5 and 1:2. The well-known 2-parameter Weibull and Exponential distributions were first fitted to the experimental data to estimate the $V_{max}$. Different approaches to sample the observed distribution of wave-by-wave overtopping volumes were evaluated including a threshold method using the top 10%, 30%, and 50% of individual overtopping volumes, and a method that applies a greater weighting to the larger events. For both Weibull and Exponential distributions, the weighted method was found to be the best one providing a 23% and 17% decrease in scatter index ($SI$) values compared to the best of existing methods. To facilitate the estimation of $V_{max}$ for design purposes, a simple empirical formula was developed as a function of the dimensionless mean overtopping discharge ($q^*$) and the number of overtopping waves ($N_{ow}$). This formula with $SI = 37\%$ outperformed the distribution-based methods as well as the best of existing formulae for $V_{max}$. In the case of the normalised bias ($NBIAS$), the distribution methods underestimated $V_{max}$ by −21% (Weibull) and −31% (Exponential) whereas the new formula yielded $NBIAS = -6\%$.

## 1. Introduction

Rubble mound seawalls are one of the important components of the coastal defence system to protect coastal areas. A safe design of a seawall is of importance for coastal designers/managers because of the highly densely populated areas on the crest (promenade) or behind the structure. For a safe design, the crest level of the seawall needs to be assessed to limit the overtopping characteristics below tolerable values specified in design manuals (US Army Corps of Engineers, 2002; EurOtop, 2018). Commonly, the mean overtopping discharge, $q$ ($m^3/s/m$), is used as the main design parameter. Several studies can be found in the literature devoted to estimating $q$ on rubble mound seawalls (e. g. van Gent et al., 2007; Jafari and Etemad-Shahidi, 2011; van der Meer and Bruce, 2014; Koosheh et al., 2022). However, the largest overtopping volumes, which may be a thousand times larger than the average overtopping volume (van der Meer and Janssen, 1994), will likely cause severe damages. Hence, it is recommended to include individual overtopping parameters such as the maximum overtopping volume, $V_{max}$ ($m^3/m$), as additional design criterion (Franco et al., 1995).

Due to the random nature of individual overtopping volumes, they are typically described using statistical distributions. To achieve this, the 2-parameter Weibull distribution is commonly used which relates the distribution of individual volumes to mean overtopping discharge ($q$), the probability of overtopping ($P_{ow}$), and the storm duration. van der Meer and Janssen (1994) as well as Franco et al. (1995) initially suggested the Weibull distribution to estimate the maximum individual

* Corresponding author.
*E-mail address:* ali.koosheh@griffithuni.edu.au (A. Koosheh).

https://doi.org/10.1016/j.coastaleng.2022.104173
Received 10 February 2022; Received in revised form 23 June 2022; Accepted 1 July 2022
Available online 12 July 2022

overtopping volume, $V_{max}$. In recent decades, the application of the Weibull distribution to describe the distribution of individual overtopping volumes has been investigated by Besley (1999), Victor et al. (2012), Hughes et al. (2012), Nørgaard et al. (2013), Zanuttigh et al. (2013), Ju et al. (2019) and Mares-Nasarre et al. (2020) on a variety of structures and nearshore wave conditions. However, these previous studies are mostly limited to the studied ranges of parameters and structural type. For example, determining the Weibull shape factor ($b$) is one of the controversial issues. In the earlier studies (e. g. van der Meer and Janssen, 1994; Bruce et al., 2009), a fixed value of this parameter (e. g. $b = 0.75$) was assumed for the structures with emergent crests, while later studies showed that the parameter $b$ can be related to wave/-structural parameters or the mean overtopping discharge ($q$). Another Weibull parameter, the scale factor ($a$) can be traditionally calculated by forcing the mean value of the Weibull distribution to be equal to the mean individual overtopping volume, $\overline{V}$ ($m^3$/m). However, some studies such as Pan et al. (2016), Gallach-Sánchez (2018), and Molines et al. (2019) have recently stated that both Weibull parameters can be obtained through the measured individual overtopping volumes.

In practice, small overtopping volumes, which may not be important in terms of overtopping hazard, can affect the distribution and lead to inaccurate $V_{max}$ estimations. Hence, a portion of the highest individual volumes is usually used to fit the Weibull distribution to the data. This issue can be addressed as another challenge of individual wave overtopping studies as no unique criterion exists for selecting the threshold value to eliminate the small volumes. For example, for rubble mound breakwaters, Bruce et al. (2009) used volumes greater than the average overtopping volume to study the distribution, while Victor et al. (2012) considered the top 10% of the individual overtopping volumes for impermeable steep slopes with a smooth surface (see Koosheh et al., 2021 for details). The selection of threshold value/criterion is somehow subjective and needs better justification. Recently, Molines et al. (2019) proposed a weighted method in which the assigned weight to each volume is proportional to its value. This technique somehow overcomes the above challenge as all individual volumes are considered for the analysis, but with different weights.

In brief, existing studies of the wave by wave overtopping of rubble mound seawalls are limited and need to be revised/improved. The present paper aims to study the distribution of individual overtopping volumes at rubble mound seawalls and to improve the existing predictive tools to estimate the maximum individual overtopping volume ($V_{max}$). For this purpose, small-scale physical model tests, covering a practical range of the wave and structural parameters, were conducted to extend the experimental data available for rubble mound seawalls. The paper is organized as follows: section 2 provides a review of the literature; sections 3 and 4 provide the details of experimental methodology, and the data analysis techniques used for the signal analysis and identifying individual volumes. The existing methods and formulae to estimate parameters such as the probability of overtopping ($P_{ow}$) and $V_{max}$ are evaluated in section 5 which also includes the development of a new and improved formulation to estimate $V_{max}$. Finally, section 6 presents the summary and conclusions of this research.

## 2. Literature review

### 2.1. Distribution of individual overtopping volumes

The probability distribution of individual overtopping volumes can be described by sorting overtopping volumes in descending order. The exceedance probability of each volume is expressed as (Su et al., 1992):

$$\widehat{P}_v = \frac{i}{N_{ow}+1} \tag{1}$$

where $N_{ow}$ is the number of overtopping waves, and $i$ is the rank of an individual volume. The Weibull distribution was initially proposed (e. g. Franco et al., 1995; van der Meer and Janssen, 1994) to analyze the individual overtopping volumes at coastal structures. Accordingly, the exceedance probability of an individual volume can be represented as:

$$P_v = \exp\left[-\left(\frac{V_i}{a}\right)^b\right] \tag{2}$$

where $a$ and $b$ are known as Weibull scale and shape factors respectively, $V_i$ is the individual overtopping volume. The non-dimensional factor $b$ adjusts the shape of the distributions and $a$ normalizes the distribution. By assuming that the theoretical and measured average overtopping discharge are equal (perfect Weibull fit of the data), $a$ and $b$ can be related as:

$$a = \frac{1}{\Gamma\left(1+\frac{1}{b}\right)}\frac{qT_m}{P_{ow}} \tag{3}$$

where $q$ is the mean overtopping discharge ($m^3$/s/m), $T_m$ is the mean wave period, and $P_{ow}$ is the probability of overtopping i.e., the ratio of the number of overtopping waves to the number of incident waves ($N_w$). Here, $\Gamma$ stands for the mathematical gamma function:

$$\Gamma(x) = \int_0^\infty t^{x-1}e^{-t}dt \tag{4}$$

van der Meer and Janssen (1994) suggested following Eq. (5) to estimate the maximum individual overtopping volume $V_{max}$:

$$V_{max} = a\left[\ln(N_{ow})\right]^{1/b} \tag{5}$$

To avoid the inconsistency for $N_{ow} = 1$ (leading to $V_{max} = 0$), Lykke Andersen et al. (2009) proposed:

$$V_{max} = a\left[\ln(N_{ow}+1)\right]^{1/b} \tag{6}$$

The earliest studies of individual wave overtopping volumes at coastal structures (e. g. Franco et al., 1995; van der Meer and Janssen, 1994) suggested a constant value of 0.75 for $b$. This low value used for common coastal structures with an emergent crest indicates that most of the overtopping volumes are relatively small, and that only a small portion of the volumes is considerably larger than the average value (Victor et al., 2012). On the other hand, when $b$ becomes larger, overtopping volumes are more evenly distributed which could be the case for structures with a low or submerged crest (Koosheh et al., 2021). For sloped structures, Besley (1999) investigated the effect of wave steepness on the Weibull shape factor and suggested $b = 0.76$ and $b = 0.92$ for wave steepness of $s_{op} = 0.02$ and 0.04, respectively. Bruce et al. (2009) studied the distribution of individual overtopping volumes on breakwaters with the different armour types and $0.8 \leq R_c/H_{m0} \leq 1.3$ where $R_c$ is the crest freeboard, and $H_{m0}$ is the spectrally derived significant wave height. The authors used individual overtopping volumes greater than the mean value and suggested the average value of 0.74 for the Weibull shape factor while no clear relation was reported between that parameter and the armour type.

Victor et al. (2012) conducted a more detailed analysis on the distribution of individual overtopping volumes at smooth sloped structures with $0.1 \leq R_c/H_{m0} \leq 1.69$. Using the highest 50% of individual volumes, they found an exponentially decreasing trend of shape factor $b$ which leads to the high $b$ values for the lower values of the relative crest freeboard. Finally, by establishing a linear trend between shape factor and the slope of structure, Victor et al. (2012) suggested:

$$b = \exp\left(-2.0\frac{R_c}{H_{m0}}\right) + 0.15\cot\alpha + 0.56 \tag{7}$$

Zanuttigh et al. (2013) analysed the Weibull shape factor for smooth and rough sloped structures with a wide range of the relative crest freeboard ($-2 \leq R_c/H_{m0} \leq 3.2$) including both small and large-scale data collected in different studies. They stated that relating the shape factor

to wave and structural parameters (e. g. relative crest freeboard) results in large scatter in the data, especially for rubble mound structures. As an alternative method, the Weibull shape factor was directly related to a dimensionless mean overtopping discharge ($\frac{q}{gH_{m0}T_{m-1,0}}$):

$$b = 0.85 + 1500\left(\frac{q}{gH_{m0}T_{m-1,0}}\right)^{1.3} \quad (8)$$

where $g$ is the acceleration due to gravity and $T_{m-1,0}$ is the spectral wave period. This equation assumes a fixed value of $b = 0.85$ for low overtopping discharges (say $\frac{q}{gH_{m0}T_{m-1,0}} < 10^{-3}$), while for high discharge values, the Weibull shape factor increases sharply.

Nørgaard et al. (2013) investigated the distribution of individual overtopping volumes at conventional breakwaters in depth-limited breaking wave conditions. They conducted small-scale physical tests with $0.9 \le R_c/H_{m0} \le 2$, cot $\alpha = 2$, $0.18 \le H_{m0}/h \le 0.55$ where $h$ is the water depth at the toe of the structure. By using the highest 50% of individual volumes, they suggested:

$$b = \begin{cases} 0.75 & \frac{H_{m0}}{h_t} \le 0.2 \quad or \quad H_{m0} \Big/ H_{\frac{1}{10}} \le 0.848 \\ -6.1 + 8.08\frac{H_{m0}}{H_{1/10}} & \frac{H_{m0}}{h_t} > 0.2 \; and \; H_{m0} \Big/ H_{\frac{1}{10}} > 0.848 \end{cases} \quad (9)$$

where $H_{1/10}$ is the average of the highest 10% of incident waves.

Molines et al. (2019) analysed the data collected by Smolka et al. (2009) on breakwaters with a crown wall in non-breaking wave conditions with $1.2 \le R_c/H_{m0} \le 4.78$ and $P_{ow} < 0.2$. Based on the findings of some recent researches (e. g. Gallach-Sánchez, 2018; Pan et al., 2016) that the Weibull parameters may not be related as stated in Eq. (3), Molines et al. (2019) proposed:

$$b = 0.63 + 1.25\exp\left(-3\times10^5\frac{q}{gH_{m0}T_m}\right) \quad (10)$$

$$A = 1.4 - \frac{0.4}{b} \quad (11)$$

where

$$A = \frac{aP_{ow}}{qT_m} \quad (12)$$

They argued that using only the upper part of the individual overtopping volume distribution and specifying a threshold to discard the low values is not easy to justify. The authors defined a weighted method, called the quadratic utility function, in which the weight applied to each overtopping volume is:

$$w_i = \left(\frac{V_i}{V_{max}}\right)^2 \quad (13)$$

where $i$ is the rank. In this method, all individual volumes are incorporated in the analysis but larger weights are applied to the larger overtopping volumes. Molines et al. (2019) reported that by using this weighted approach, more accurate predictions of $V_{max}$ are obtained in comparison to analysing the upper part of the volume distributions (e. g. 10%, 30%, and 50%).

As an alternative method, a 2-parameter Exponential distribution was also suggested by Molines et al. (2019) to study individual overtopping volumes. Accordingly, the exceedance probability of an individual volume was expressed as:

$$P_v = \exp\left[-\left(\frac{V-c}{d}\right)\right] \quad (14)$$

where $c$ and $d$ are free parameters. The maximum individual overtopping volume is given by:

$$V_{\max} = D\overline{V}\left[\ln(N_{ow}+1) + C/D\right] \quad (15)$$

where $C = c/\overline{V}$ and $D = d/\overline{V}$ are dimensionless parameters and $\overline{V}$ is the mean overtopping:

$$\overline{V} = \frac{qT_mN_w}{N_{ow}} \quad (16)$$

Using the weighted method, the following exponential distribution for mound breakwaters with the crown wall was suggested as:

$$D = 2.6 - 2.6\exp\left(-3\times10^5\frac{q}{gH_{m0}T_m}\right) \quad (17)$$

$$C = 1.2 - D - 0.2D^2 \quad (18)$$

Later, Mares-Nasarre et al. (2020) followed Molines et al. (2019)'s methodology and recalibrated Eqs. (10) and (11) for mound breakwaters in breaking wave conditions with $0.33 \le R_c/H_{m0} \le 2.83$ and $0.2 \le H_{m0}/h \le 0.9$ and obtained:

$$b = 0.8 + \exp\left(-2\times10^5\frac{q}{gH_{m0}T_m}\right) \quad (19)$$

$$A = 1.5 - \frac{0.4}{b} \quad (20)$$

The existing empirical formulae in the literature to estimate $V_{max}$, summarized in Table 1, are mostly out of range of the present study's scope which focuses on structures with an impermeable core and without wave-wall in non-breaking wave conditions (Fig. 1).

### 2.2. Probability of overtopping and number of overtopping waves

As discussed above, the study of the distribution of individual overtopping volumes requires the estimation of the number of overtopping waves, $N_{ow}$. This parameter can be estimated from the probability of overtopping, $P_{ow} = N_{ow}/N_w$. For rubble mound structures with $1 \le$ cot $\alpha \le 2$, Owen (1980) first proposed:

$$P_{ow} = \exp\left(K_1\left(\frac{1}{\gamma_f}\frac{R_c}{T_m\sqrt{gH_{m0}}}\right)^2\right) \quad (21)$$

where $K_1$ is 63.8 and 37.8 for the slope of cot $\alpha = 1$ and 2, respectively. van der Meer and Janssen (1994) correlated the probability of overtopping to the relative crest freeboard ($R_c/H_{m0}$) and suggested (EurOtop, 2018 – Eq. (5.56)):

$$P_{ow} = \exp\left(-\left(\frac{1}{\chi}\frac{R_c}{H_{m0}}\right)^2\right) \quad (22)$$

**Table 1**
Summary of existing the formulae to estimate $V_{max}$ (sloped structures).

| Author | Structure type | $R_c/H_{m0}$ | cot $\alpha$ | $h/H_{m0}$ | Wave wall |
|---|---|---|---|---|---|
| van der Meer and Janssen (1994) | Impermeable | – | – | – | No |
| Victor et al. (2012) | Smooth - impermeable | 0.10–1.69 | 0.36–2.75 | 2.70–25 | No |
| Zanuttigh et al. (2013) | Smooth & Rough | 0.00–1.65 | 2–4 | – | – |
| Nørgaard et al. (2013) | Rough - impermeable | 0.90–2.00 | 1.5 | 2–5.55 | Yes |
| Gallach-Sánchez (2018) | Smooth - Steep slopes | 0.00–3.25 | 0–2 | 2–33 | No |
| Molines et al. (2019) | Rough - permeable | 1.20–4.78 | 1.5 | 3.12–10 | Yes |
| Mares-Nasarre et al. (2020) | Rough - permeable | 0.33–2.83 | 1.5 | 1.11–5 | No |

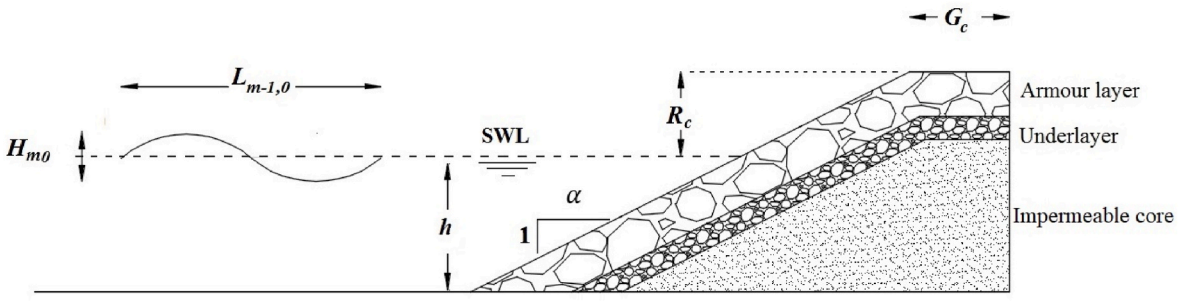


**Fig. 1.** Schematic diagram of a rubble mound seawall (Koosheh et al., 2022).

The coefficient $\chi$ can be calculated as:

$$\chi = \frac{1}{\sqrt{-ln(0.02)}} \frac{R_{u2\%}}{H_{m0}} \tag{23}$$

where $R_{u2\%}/H_{m0}$ is the dimensionless run-up height exceeded by 2% of incident waves and is estimated as:

$$\frac{R_{u2\%}}{H_{m0}} = 1.5\gamma_h\gamma_f\gamma_\beta Ir_p \leq 3\gamma_h\gamma_f\gamma_\beta \tag{24}$$

Here, $\gamma_h$, $\gamma_f$ and $\gamma_\beta$, with the maximum value of one, are reduction coefficients that account for the effects of shallow water conditions, the roughness, and the obliquity of the incident wave, respectively. $Ir_p$ is the Iribarren number (breaker parameter) defined as $tan\,\alpha/(s_{op})^{0.5}$ where $s_{op} = 2\,\pi\,H_{m0}/(gT_p^2)$ represents the wave steepness. Several studies have focused on improving the estimation of the coefficient $\chi$ (see TAW, 2002; EurOtop, 2007; Victor et al., 2012). EurOtop (2018) recommends Eq. (22) for the estimation of the probability of overtopping using the corrected 2% relative run-up (EurOtop, 2018 – Eq. (6.1)):

$$\frac{R_{u2\%}}{H_{m0}} = 1.65\gamma_f\gamma_\beta Ir_{m-1,0} < 1.0\,\gamma_{f\_surging}\gamma_\beta\left(4 - \frac{1.5}{\sqrt{Ir_{m-1,0}}}\right) \tag{25}$$

with the maximum value of 3 where $\gamma_{f\_surging}$ is calculated as:

$$\gamma_{f\_surging} = \gamma_f + \frac{(Ir_{m-1,0} - 1.8)(1 - \gamma_f)}{8.2} \tag{26}$$

where $Ir_{m\text{-}1,0}$ is the Iribarren number using the spectral wave period.

Recently, Molines et al. (2019) and Mares-Nasarre et al. (2020) suggested a relationship between the probability of overtopping and the dimensionless mean overtopping rate ($Q^* = q/gT_mH_{m0}$) and proposed Eqs. (27) and (28) for mound breakwaters in deep-water and depth-limited conditions respectively as:

$$P_{ow} = 480Q^{*0.8} \tag{27}$$

$$P_{ow} = \exp\left(-\frac{0.1}{Q^{*0.3}}\right) \tag{28}$$

In summary, the estimation of $P_{ow}$ using the most common form (Eq. (22)) relies on the accuracy of the run-up estimation which, itself, depends on structural and wave characteristics.

## 3. Physical model test

### 3.1. Experiment set up

Two-dimensional (2D) small-scale physical model tests were carried out in the hydraulics laboratory of Griffith University. The wave flume is 22.5 m long, 0.8 m deep and 0.5 m wide and has a piston-type wavemaker. The wave generation system is capable of generating both regular and irregular waves and equipped with a dynamic wave absorption system to reduce the effect of reflected waves from the structure. To measure free water surface elevation and estimate wave parameters, three capacitance wave gauges (WG1, WG2, and WG3) were placed near the toe of the structure (see Fig. 2). Incident and reflected waves were separated using the three-probe method proposed by Mansard and Funke (1980). The possible effect of low frequency (infra-gravity) waves on water surface fluctuations was checked by analysing the observed water levels and no significant low-frequency oscillation was found.

The selection of the seawall model section was based on Koosheh et al. (2022)'s analysis of the existing database which identified a data gap for slopes cot $\alpha \leq 2$. Hence, a 2-layer seawall with the slopes of 1:2 and 1:1.5 was selected for this study. The rubble mound seawall model consisted of an armour layer ($D_{n50}$ = 38 mm) and a filter layer ($D_{n50}$ = 17 mm) obtained from the stability formula of Etemad-Shahidi et al. (2020). The impermeable core, as the most common case for seawalls, was made of plywood timber with surface friction enhanced using glue and sand. The rock layers with a minimum layer thickness of $2D_{n50}$ were placed on the timber slope.

To capture the overtopped water, a horizontal acrylic sheet was used to cover the crest and was sealed at the flume's walls to prevent leakage. The overtopped water was collected via a small chute, with a length of 250 mm and a width of 66 mm, into a rectangular box placed behind the seawall (Fig. 2). To avoid the influence of possible boundary effects from the flume's walls on the overtopped flow, the chute was placed at the centre of the flume. No significant deviation of the trajectories of the overtopping waves and no effect of wave gauges on overtopped flow on the smooth crest was observed during the tests. The maximum difference of 0.5% between the total collected volume in the box and the sum of individual overtopping volumes during an individual test confirms that very small overtopping volumes have been measured with an acceptable accuracy.

The wave-by-wave measurement of overtopping volumes was achieved by reading the water surface level inside the box. For this purpose, two wave gauges (WG6 and WG7), with the initial submergence depth of 100 mm, were installed at the opposite corners of the box, and their average readings were used to calculate the overtopping volume. To reduce the water surface fluctuations due to the overtopping, especially large events, a stilling wall was placed inside the box (Fig. 3). The number of overtopping waves ($N_{ow}$) is not easy to measure based on the records of the wave gauges inside the box (Koosheh et al., 2021). This is because the small overtopping events may not be identified when they reach the box immediately before/after a large overtopping event. Hence, two wave gauges (WG4 and WG5) were installed on the seaward edge and the middle of the crest (250 mm distance) to detect overtopping events (the details of coupling the wave gauges on the crest with those installed inside the box to analyze the water level data will be discussed in section 4.2). Since the wave gauges on the crest of the seawall need to be kept partially submerged during the experiment, a 10-L rectangular box full of water was installed beneath the crest (see Figs. 2 and 3), and the wave gauges pierced inside the box via holes on the crest's surface. The water level inside the box, which normally should be the same as the crest level, was regularly checked to avoid any effect on small overtopping events passing the crest. Signals received

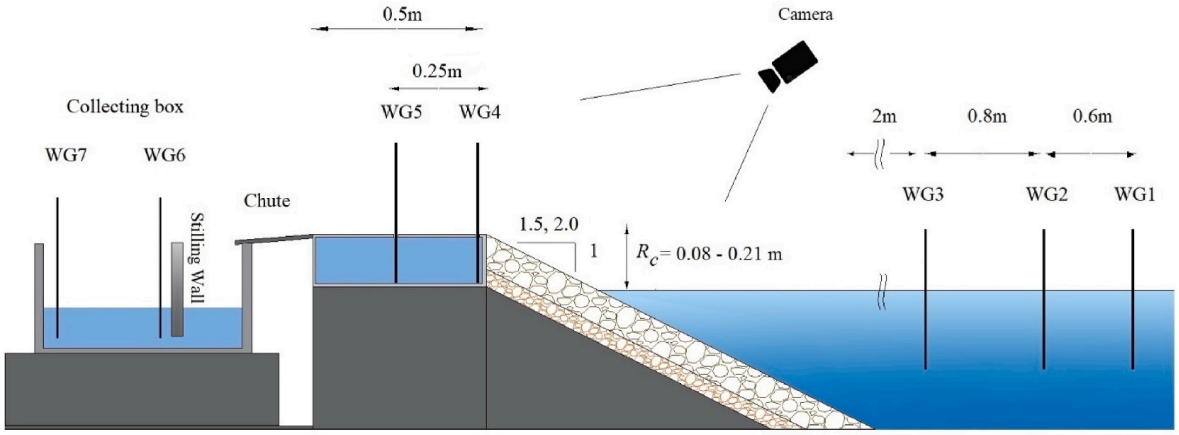


**Fig. 2.** Measurement instruments and the cross-section of seawall model.

from the probes were recorded by the National Instruments data acquisition card and MATLAB script (home-developed) at the frequency of 20 Hz. Two high-speed cameras were deployed above and beside the tank to supplement and quality control the wave gauge data during post-processing.

### 3.2. Test programme

A total of 135 tests were carried out on the rubble mound seawall model with slopes of 1:1.5 (67 tests) and 1:2 (68 tests). Each test consisted of approximately 1000 irregular waves generated based on a JONSWAP spectrum with peak enhancement factor $\gamma = 3.3$. The spectral significant wave height ($H_{m0}$) and peak wave period ($T_p$) were obtained from the incident waves near the toe of the structure. Table 2 provides the details of the measured parameters for the present study. For the design of the experiments, using the EurOtop (2018) formula (see Appendix A), a preliminary estimation of the mean overtopping discharge $q$ ($m^3/s/m$) was performed to ensure $q > 10^{-6}$. This is because very low values of the mean overtopping discharge may be affected by measurement errors and/or scale effects (van Gent et al., 2007; Shaeri and Etemad-Shahidi, 2021). The relative crest freeboard values were kept within the practical range of $0.75 \leq R_c/H_{m0} \leq 2.5$ and all tests were conducted in deep water conditions, i.e. $h/H_{m0} > 3$ (Ciria, 2007; Shaeri and Etemad-Shahidi, 2021). The range of the Iribarren number ($Ir_{m\text{-}1,0}$) with a minimum of 2.17 shows that the present study covers only non-breaking waves at the structure slope, which is common for rubble mound structures (EurOtop, 2018).

## 4. Data processing and analysis

### 4.1. Measurement of the number of overtopping waves ($N_{ow}$)

Accurate determination of the number of overtopping waves is crucial as it affects the distribution of individual overtopping volumes and consequently the estimation of $V_{max}$. The detection of a small overtopping event is quite challenging through the recorded signals in the collecting box, especially if they arrive immediately after a large event (Molines et al., 2019). As mentioned before, two wave gauges were placed on the crest of the seawall model (the seaward edge, and the middle) to detect the overtopping events. Indeed, these wave gauges record the continuous reading (time series) of the overtopping flow thickness (depth), $h_c$, at a particular point. A time-domain threshold-down-crossing algorithm was applied to identify the occurrence of the overtopping events using the recorded signals. This algorithm is based on specifying a fixed threshold ($r_s$) value for each recorded signal. The appropriate selection of the threshold needs to be customized based on the signal's nature, structural and wave characteristics (Formentin and Zanuttigh, 2019; Koosheh et al., 2021).

Near the seaward edge of the crest, water splash (due to wave impact at the crest) may cause the wave gauge not to return a signal consistent with a real overtopping event. To overcome this issue, the coupling method proposed by Formentin and Zanuttigh (2019) was used which assumes that a single overtopping event, traveling over the crest, should be recorded by both probes but with a delay that depends on the distance between the probes and the wave celerity. This method was applied as follows:

First, the threshold down-crossing algorithm was applied to both records of the wave gauges installed on the crest of the structure, and overtopping events were determined. It should be mentioned that overtopping flow thickness decreases along the crest (van Gent, 2002; Schüttrumpf and van Gent, 2003). This means that an overtopping event has its highest thickness on the seaward edge of the crest and by moving toward the lee side, its thickness decreases gradually. Hence, due to the higher overtopping thickness values at WG4 (seaward edge) in comparison to WG5 (middle of the crest), the specified threshold of WG5 needs to be low enough (equal or lower than that of WG4) to detect small overtopping events. Fig. 4 shows the recorded signals from the probes on the crest of the structure with specified threshold values.

The second step is comparing the two signal outputs from step one to ensure that an overtopping event detected at the first probe (WG4), is also detected at the second probe (WG5). If not, then the event was discarded. The acceptable time lag between the instants of detection of a single event at two probes can be defined as:

$$dt_{min} = \max\left(\frac{d_w}{c_d}, \frac{1}{S_f}\right) \tag{29}$$

$$dt_{max} = \frac{d_w}{c_s} \tag{30}$$

where $c_d$ stands for the maximum wave celerity defined by $L_{0p}/T_p$, and $d_w$ is the distance between two wave gauges in the direction of the overtopping. The parameter $S_f$ is the sampling rate which is recommended to be more than $c_d/d_w$. The minimum possible celerity ($c_s$) can be defined as a function of minimum measured flow thickness at the first wave gauge ($h_{Cmin}$):

$$c_s = \sqrt{g h_{Cmin}} \tag{31}$$

Paired events with time lags outside of the acceptable range [$dt_{min}$, $dt_{max}$] were discarded. For example, for the test given in Fig. 4, with $T_p$ = 1.89 s, $S_f$ = 20 Hz, and $h_{cmin}$ = 0.003 m, the acceptable range of delay between two wave gauges is [0.05s, 0.8s]. To assess the accuracy of the applied technique to detect overtopping events, for some randomly selected tests, the number of overtopping events was determined

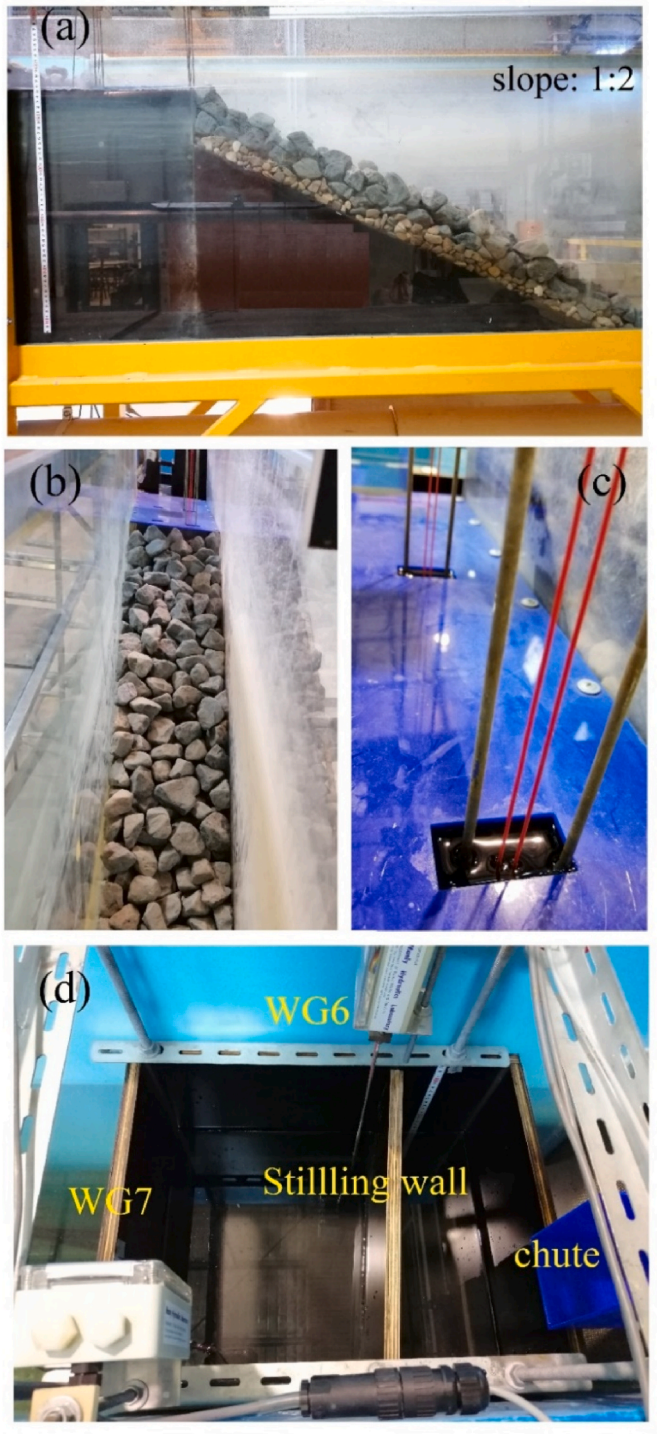


**Fig. 3.** (a) and (b): front view of the seawall model; (c): Pierced wave gauges WG4 (closer) and WG5 (further) on the crest (view from the seaward side); (d): top view of overtopping collecting box.

manually using the recorded videos. The comparison of results of the manual calculation with those of the coupling method (automatic approach) showed that the differences between obtained $N_{ow}$ values were below 2%.

### 4.2. Wave-by-wave measurement of overtopping volumes

Individual overtopping volumes were determined based on the changes in water depth in the collecting box computed based on the average of the two wave gauges (WG6 and WG7). A stilling wall inside the box helped to reduce the water surface fluctuations induced by each overtopping event. Some noise persisted in the raw gauge signal, especially when large overtopping events discharged into the box, so moving average and low pass filters were applied to further de-noise the signals.

**Table 2**
Ranges of measured key parameters for the conducted tests.

| Parameter | Range | |
|---|---|---|
| | Slope 1:1.5 | Slope 1:2 |
| $R_c$ (m) | 0.08–0.21 | 0.10–0.18 |
| $H_{m0}$ (m) | 0.07–0.13 | 0.07–0.13 |
| $T_{m-1,0}$ (s) | 1.07–1.94 | 1.08–1.96 |
| $T_p$ (s) | 1.18–2.13 | 1.19–2.16 |
| $h$ (m) | 0.35–0.48 | 0.38–0.46 |
| $q$ ($m^3$/s/m) | $1.53 \times 10^{-6}$–$8.48 \times 10^{-4}$ | $2.30 \times 10^{-6}$–$1.35 \times 10^{-3}$ |
| $R_c/H_{m0}$ | 0.8–2.5 | 0.75–2.02 |
| $cot\ \alpha$ | 1.5 | 2 |
| $s_{m-1,0}$ | 0.014–0.056 | 0.014–0.052 |
| $Ir_{m-1,0}$ | 2.81–5.38 | 2.17–4.19 |
| $h/H_{m0}$ | 3.20–6.66 | 3.43–6.06 |
| Number of data points | 67 | 68 |

For the accurate determination of individual overtopping volumes, overtopping events first need to be carefully detected. The output signal, known as the Cumulative Volume Curve (CVC, see Fig. 5), represents the history of overtopped volume inside the collecting box during a test and any sudden increase (jumps) in water volume (or level) indicates the occurrence of an overtopping event (Franco et al., 1995). A preliminary analysis was performed to recognize individual overtopping volumes automatically using an algorithm based on the detection of the sudden increases of the mean value of the CVC. As the automatically detected jumps do not necessarily correspond to a real, individual overtopping event due to signal complexity (Hughes and Thornton, 2016), the coupled detection method (used above) was also applied to the CVC using the wave gauges installed on the crest (the output of section 4.1). This assumes that each overtopping event detected in the CVC (inside the collecting box) should also be detected by the wave gauges on the crest a few seconds earlier (pairing process).

Fig. 5 shows the coupling of the overtopping cumulative volumes curve (CVC) with the recorded signals from WG4 (crest) for a typical test. Five overtopping events were detected in the signal sample shown based on the wave gauge installed on the crest (dashed curve). The corresponding pairs of those five events can be seen as the sudden increases in the CVC (solid curve). The times of the sudden increases are shown as $t_i$ where $i$ represents the counter id of overtopping events. As seen, there is about a 1 s delay between the detection of an overtopping event on the crest (seaward edge) and the corresponding volume increase in the collecting box which is the travel time of the overtopped water (to pass the crest, chute and stilling wall). Each overtopping volume can be calculated as the difference between the CVC values recorded at two consecutive sudden increase points ($V_c$):

$$V\ (i) = V_c\ (t_{i+1}) - V_c(t_i) \tag{32}$$

In the case of complex signals that typically occur during low-crested tests or consecutive large events, the recorded signal was manually checked and corrected (if needed) to ensure the overtopping volumes were determined accurately. The small peaks observed after the main peaks (e. g. events no.4 and 5), could be due to the water splash at the seaward edge of the crest which are discarded by the abovementioned algorithms.

$V_{max}$ is the highest individual overtopping volume recorded within a test. Since the tests contain 1000 waves, $V_{max}$ can also be regarded as the volume that can be exceeded by less than 0.1% of the incident waves ($V_{0.1\%}$). For a peak of a storm that is characterised by 1000 waves, $V_{max}$

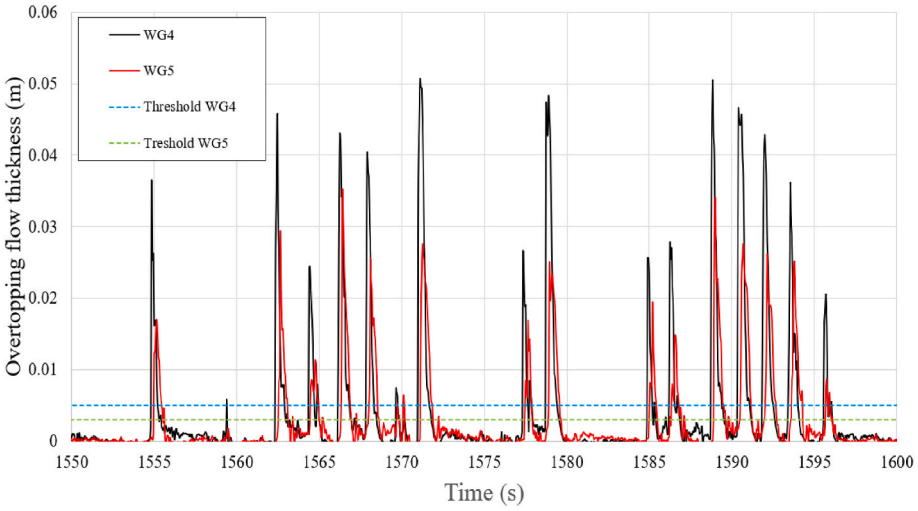


**Fig. 4.** Recorded time series from the wave gauges installed on the crest of the seawall ($h$ = 0.46 m, $H_{m0}$ = 0.09 m, $T_p$ = 1.89 s).

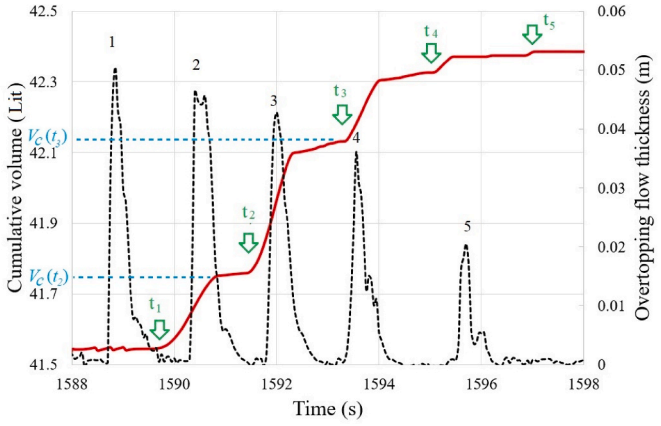


**Fig. 5.** Coupling cumulative volume curve (solid) with recorded signal from the wave gauge installed on the crest (WG4: dashed), $h$ = 0.46 m, $H_{m0}$ = 0.09 m, $T_p$ = 1.89 s.

is the real maximum volume per individual wave overtopping event.

## 5. Results and discussion

### 5.1. Estimation of $P_{ow}$ and $N_{ow}$

To evaluate the goodness of fit between the estimated and measured values, the Normalised Bias (*NBIAS*) and Scatter Index (*SI*) were used as below:

$$NBIAS = \frac{1}{E_{mea,av}} \left( \frac{1}{n} \sum_{i=1}^{n} \left[ E_{est,i} - E_{mea,i} \right] \right) \tag{33}$$

$$SI = \frac{1}{E_{mea,av}} \sqrt{\frac{1}{n} \sum_{i=1}^{n} \left\{ \left[ E_{est,i} - E_{mea,i} \right]^2 \right\}} \tag{34}$$

where $n$ is the number of records, $E_{est,i}$ and $E_{mea,i}$ are the estimated and measured values, respectively. $E_{mea,av}$ stands for the average of measured values. *NBIAS*, with zero value for a perfect estimation, is used to calculate the average difference between measured and estimated values. On the other hand, *SI*, as a non-negative metric, quantifies the scatter of the estimation. The given accuracy metrics (Eqs. (33) and (34)) are the normalised forms of well-known metrics namely *bias* and *RMSE*.

Table 3 compares the skill of the existing formulae (section 2.2) for the estimation of the probability of overtopping ($P_{ow}$). Although all formulae overestimated the observed values (*NBIAS* > 0), the EurOtop (2018) formula with the lowest *SI* (= 51%) outperformed others.

Fig. 6 shows the scatter plot of measured against estimated $N_{ow}$ using different formulae. Estimated values of $N_{ow}$ were obtained through $P_{ow} = N_{ow}/N_w$, based on the measured $N_w$ and corresponding estimated $P_{ow}$. The EurOtop (2018) formula is seen to be the best estimator of $N_{ow}$ and is, therefore, the one chosen to be used for further analysis regarding the estimation of $V_{max}$ (following sections).

### 5.2. Estimation of $V_{max}$ using the existing formulae

The $V_{max}$ formulae described in section 2.1, try to find the best fit to the distribution of individual overtopping volumes by adjusting some parameters (e. g. shape and scale factors in Weibull distribution). These parameters, themselves, are a function of different parameters such as the mean overtopping discharge ($q$), the number of overtopping waves ($N_{ow}$), and wave and structural features (e. g. $R_c/H_{m0}$, cot $\alpha$).

In practice, when designing a seawall, the design wave conditions (e. g. $H_{m0}$, $T_{m-1,0}$) and structural geometry are given, however, $q$ and $N_{ow}$ are unknown. Hence, these two parameters are required to estimate the $V_{max}$ value. The performance of the existing formulae for the estimation of $N_{ow}$ was discussed above and the expression proposed in EurOtop (2018) was found the best one. The estimation of $q$ using predictive tools is commonly associated with large errors (Koosheh et al., 2020) which can greatly affect the estimation of $V_{max}$. Recently, Koosheh et al. (2022) conducted laboratory experiments and analysed the skill of the existing empirical formulae to estimate $q$. They reported that the EurOtop (2018) formula underestimates $q$ significantly as it has not been trained optimally, especially for long waves (low wave steepness). Hence, by including the effect of wave steepness, they proposed an improved formula using their own collected data and those of the existing database for rubble mound seawalls as below:

**Table 3**
Estimation of the probability of the overtopping ($P_{ow}$) using existing formulae.

| Formula | *NBIAS* (%) | *SI* (%) |
|---|---|---|
| van der Meer and Janssen (1994) | 16 | 59 |
| Owen (1980) | 63 | 95 |
| EurOtop (2018) | 24 | 51 |
| Molines et al. (2019) | 25 | 59 |
| Mares-Nasarre et al. (2020) | 24 | 61 |

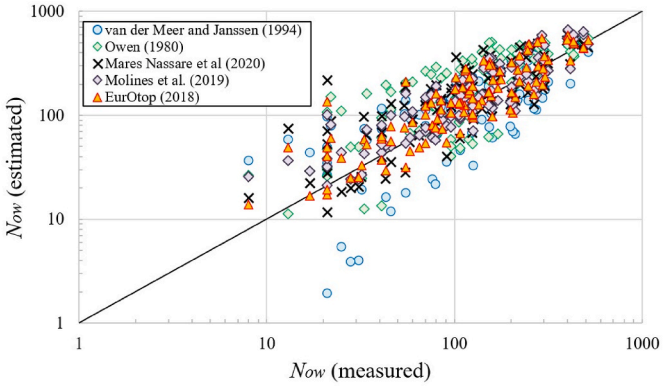


**Fig. 6.** Measured against estimated $N_{ow}$ using different existing formulae.

$$\frac{q}{\sqrt{gH_{m0}^3}} = 0.034 \exp\left[-4.97\left(\frac{R_c}{H_{m0}\cdot\gamma_f}\right)^{1.12}\left(s_{m-1,0}\right)^{0.35}\right] \quad (35)$$

Table 4 compares the accuracy of the existing formulae and the best performing of the present study to estimate the non-dimensional $V^*_{max}$ ($\frac{V_{max}}{gHm0T_m^2}$) with both the estimated and measured values of $N_{ow}$ and $q$. For the existing formulae, the estimated values of $N_{ow}$ and $q$ are obtained from formulae as proposed by the original authors (see Appendix B for details); and for the formulae proposed in the present study, the best estimators of $N_{ow}$ (Eqs. (22), (23) and (25)) and $q$ (Eq. (35)) were used. As expected, all formulae show better performance (average improvements of 20% and 14% in terms of *NBIAS* and *SI* respectively) when the measured values of $N_{ow}$ and $q$ are used. However, it should be noted that in practice, the measured values are not available and only the estimation of $V^*_{max}$ using the estimated $N_{ow}$ and $q$ can be used. All the existing formulae underestimate $V^*_{max}$, and the Molines et al. (2019) formula derived for non-breaking wave conditions based on the Exponential distribution, outperforms others with *NBIAS* = −52% and *SI* = 75%. It is worth mentioning that most of the formulae, such as Molines et al. (2019) and Mares-Nasarre et al. (2020), are derived for conventional mound breakwaters with a permeable core, and thus are only applied to get information, although they are not directly applicable (see Table 1).

### 5.3. Improved formulation to estimate $V_{max}$ using Weibull distribution

To improve the formulations, first, a 2-parameter Weibull distribution was fitted to the measured individual overtopping volumes and their corresponding shape and scale factors were obtained. Eq (2) can be expressed as:

$$log\ Vi = log\ a + \frac{1}{b}\log\left(-\ln P_v\right) \quad (36)$$

By fitting a line on the scatter plot with the horizontal axis of *log* (-ln ($\widehat{P}_v$)) and the vertical axis of *log* ($V_i$), parameters $a$ and $b$ can be obtained (See Fig. 7). Here, $V_i$ is the individual overtopping volume (sorted in descending order) and $\widehat{P}_v$ is estimated using Eq (1).

Different scenarios including using only 10%, 30%, and 50% of the highest individual overtopping volumes, as well as the weighted method were tested. Then, the relationship between the measured dimensionless mean overtopping discharge $q^*$ ($q/\sqrt{gH_{m0}^3}$) and obtained shape factor values ($b$) was investigated (Fig. 8a). The fitted function, with almost fixed $b$ values for the low $q^*$ and increasing trend for the higher discharges ($q^* > 10^{-3}$), matches the suggested formulae in the literature (e.g. Zanuttigh et al., 2013). In Fig. 8a, the scatter of the data is relatively large (standard deviation, $\sigma = 0.15$) in which uncertainties may contribute to the estimation of $V_{max}$. Finally, using $A = aP_{ow}/(qT_m)$, a linear formula for Weibull scale factor ($a$) was derived (Fig. 8b).

The details of the derived equations and the accuracy metrics of the estimation of $V^*_{max}$ are given in Table 5. It should be mentioned that for the estimation of $V^*_{max}$, the estimated values of $N_{ow}$ (Eqs. (22), (23) and (25)) and $q^*$ (Eq. (35)) were used. As seen, the weighted method (Model W1) with *NBIAS* = −21% and *SI* = 52% provided the most accurate estimation of $V^*_{max}$ (using Eq. (6)) which is consistent with the recent results of Molines et al. (2019) and Mares-Nasarre et al. (2020). Comparison of Models W2, W3, and W4 shows that the more data excluded from the analysis, the less accuracy is obtained. Model W1 showed 31% and 23% improvements in *NBIAS* and *SI* values, respectively compared to the formula by Molines et al. (2019) as the best of existing ones.

### 5.4. Improved formulation to estimate $V_{max}$ using exponential distribution

Using Eqs. (14) and (15), a 2-parameter Exponential distribution was fitted to the distribution of individual overtopping volumes to estimate $V^*_{max}$. For each test, the dimensionless parameters $C$ and $D$ were obtained by fitting a line to the plot with the horizontal axis of *-log* ($P_v$) and the vertical axis of $Vi/\overline{V}$ in which $\overline{V}$ stands for the average of individual overtopping volumes. The parameter $D$ was correlated to the measured dimensionless mean overtopping discharge ($q^*$) through a power function (Fig. 9a) first ($\sigma = 1.35$). Then, parameter $C$ was obtained based on parameter $D$ using a linear fit (Fig. 9b). Similar to the previous section, different scenarios using only 10%, 30%, and 50% of the highest individual overtopping volumes, and the weighted method were tested.

Obtained values of parameters $C$, $D$, and the accuracy metrics of the estimation of $V^*_{max}$ using the developed models are given in Table 6. For the estimation of $V^*_{max}$ values using the Exponential distribution, the estimated values of $N_{ow}$ (Eqs. (22), (23) and (25)) and $q^*$ (Eq. (35)) were used. Again, the weighted method (Model E1), with *NBIAS* = −31% and

**Table 4**
Accuracy metrics of formulae in the literature for the estimation of $V^*_{max}$ ($\frac{V_{max}}{gHm0T_m^2}$) using the measured and estimated values of $N_{ow}$ and $q$.

| Formula | Measured $q$ and $N_{ow}$ | | Estimated $q$ and $N_{ow}$ | |
|---|---|---|---|---|
| | *NBIAS* (%) | *SI* (%) | *NBIAS* (%) | *SI* (%) |
| van der Meer and Janssen (1994) | −51 | 71 | −68 | 84 |
| Zanuttigh et al. (2013), [a] | −56 | 77 | −68 | 85 |
| Molines et al. (2019) - Weibull | −29 | 58 | −52 | 77 |
| Molines et al. (2019) - Exponential | −27 | 56 | −52 | 75 |
| Mares-Nasarre et al. (2020) | −41 | 66 | −62 | 81 |
| Eq. (38) - (Best of the present study) | 0 | 33 | **−6** | **37** |

[a] Recommended by EurOtop (2018).

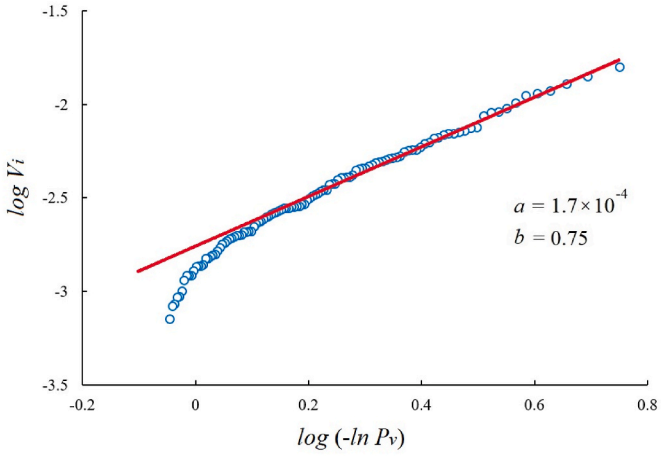


**Fig. 7.** Weibull plot (weighted fit) for a typical test ($h = 0.46$ m, $H_{m0} = 0.1$ m, $T_p = 1.59$ s).

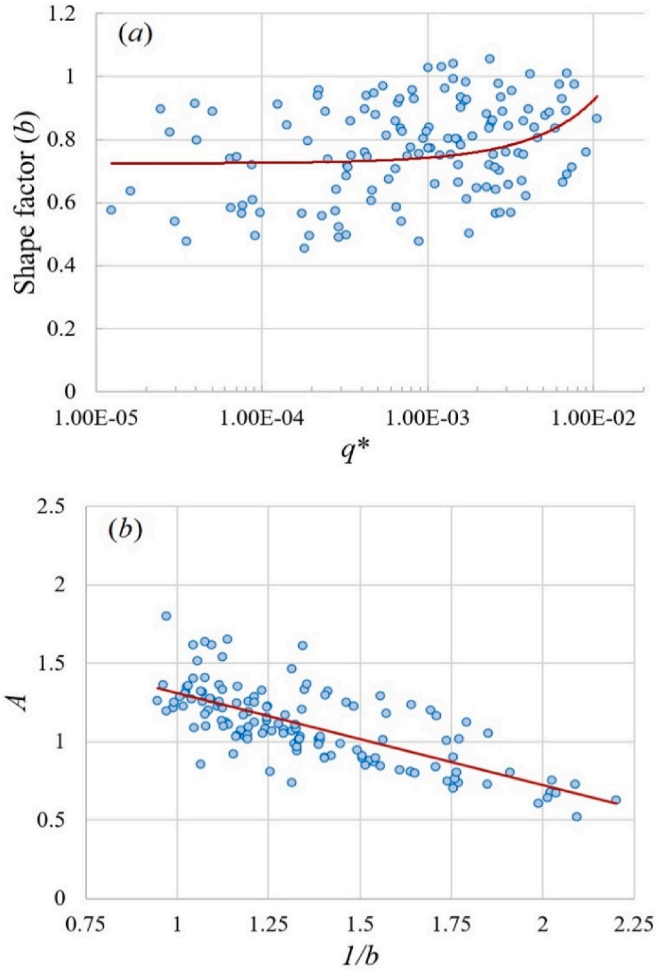


**Fig. 8.** (a) Relationship between measured dimensionless mean overtopping rate ($q^*$) and Weibull shape factor; (b): relationship between $1/b$ and A using weighted method.

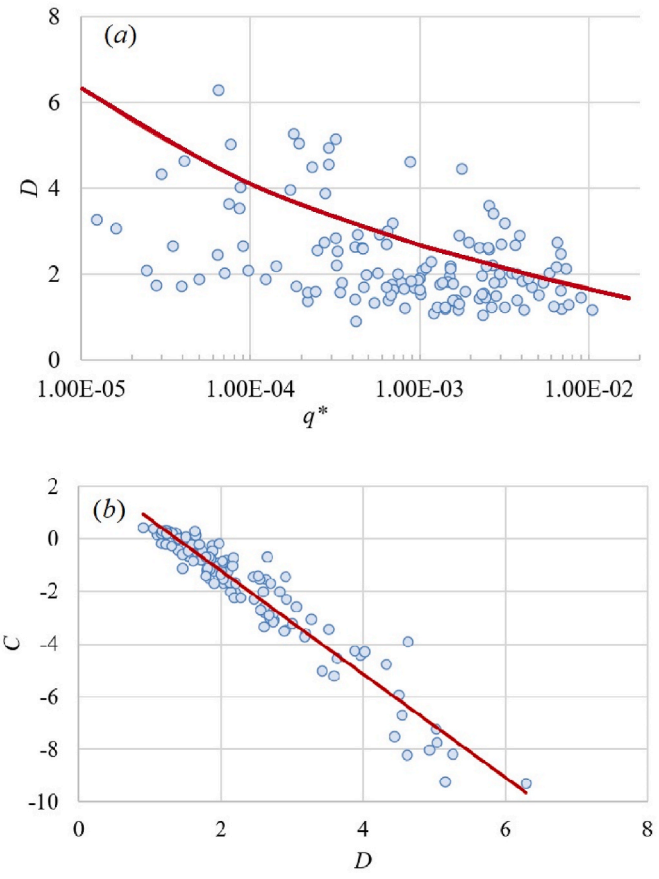


**Fig. 9.** (a) Relationship between the measured dimensionless mean overtopping rate ($q^*$) and $D$; (b) relationship between $D$ and $C$ using the weighted method (Exponential distribution).

$SI$ = 58%, outperformed other models. Model E1, as the best of the exponential distribution ones, provided 21% and 17% improvements in *NBIAS* and *SI* values compared to the formula by Molines et al. (2019) as the best of existing ones.

### 5.5. Estimation of $V_{max}$ without distribution-based methods

The existing formulations highlight the role of two key parameters namely mean $q$ and $N_{ow}$ for the estimation of $V_{max}$. In this section, the possibility of deriving a simple empirical formula to estimate $V_{max}$ without using distribution-based methods was investigated. The relationships between $V^*_{max}$ and the measured $q^*$ and $N_{ow}$ are shown in Fig. 10 where the power functional form was found to be the best fit to the data. Given that $q^* = 0$ or $N_{ow} = 0$ yields $V^*_{max} = 0$, Eq. (37) was initially proposed:

$$V^*_{\max} = a_1 \, N_{ow}{}^{a_2} \cdot q^{*a_3} \tag{37}$$

In order to achieve the best fit, a Genetic Algorithm (GA) was used to optimize the given coefficients ($a_1$, $a_2$ and $a_3$). For the optimization process, the *SI* metric (Eq. (34)) was selected as the fitness function to be minimized for the best fit as below:

$$V^*_{max} = 0.0125 \, N_{ow}{}^{0.23} \cdot q^{*0.28} \tag{38}$$

In comparison to others (Tables 5 and 6), the proposed formula (Eq. (38)) with $NBIAS = -6\%$ and $SI = 37\%$ outperformed distribution-based formulae. Estimation of $V^*_{max}$ in this way yields 15% and 21% improvements of *SI* values compared to the best Weibull and Exponential

**Table 5**

Accuracy metrics of the estimation of $V^*_{max}$ ($\frac{V_{max}}{gHm0T_m^2}$) using the different scenarios of Weibull distribution (Eq. (6)).

| Model | Used data | $b$ | A | Measured $q$ and $N_{ow}$ | | Estimated $q$ and $N_{ow}$ | |
|---|---|---|---|---|---|---|---|
| | | | | *NBIAS* (%) | *SI* (%) | *NBIAS* (%) | *SI* (%) |
| W1 | All (Weighted) | 0.722 *exp* (22.41$q^*$) | $1.8 - \frac{0.35}{b}$ | −3 | 48 | −21 | 52 |
| W2 | top 50% | 0.710 *exp* (39.59$q^*$) | $2 - \frac{0.67}{b}$ | −19 | 56 | −39 | 62 |
| W3 | top 30% | 0.810 *exp* (19.19$q^*$) | $2.68 - \frac{1.09}{b}$ | −10 | 50 | −48 | 68 |
| W4 | top 10% | 1.03 *exp* (41.03$q^*$) | $3.66 - \frac{1.75}{b}$ | −19 | 54 | −64 | 83 |

**Table 6**

Accuracy metrics of estimation of $V^*_{\max}\left(\frac{V_{\max}}{g\ Hm0T_m^2}\right)$ using different scenarios of Exponential distribution (Eq. (15)) and Eq. (38).

| Model | Used data | $D$ | $C$ | Measured $q$ and $N_{ow}$ | | Estimated $q$ and $N_{ow}$ | |
|---|---|---|---|---|---|---|---|
| | | | | *NBIAS* (%) | *SI* (%) | *NBIAS* (%) | *SI* (%) |
| E1 | All (Weighted) | $0.710\ q^{*-0.190}$ | 2.7–1.96$D$ | −4 | 52 | −31 | 58 |
| E2 | top 50% | $0.725\ q^{*-0.148}$ | 2.47–1.85$D$ | −21 | 52 | −44 | 66 |
| E3 | top 30% | $0.856\ q^{*-0.122}$ | 3.07–2.12$D$ | −17 | 56 | −46 | 66 |
| E4 | top 10% | $1.475\ q^{*-0.05}$ | 4.43–2.8$D$ | −21 | 58 | −44 | 64 |
| Eq. (38) | – | – | – | 0 | 33 | −6 | 37 |

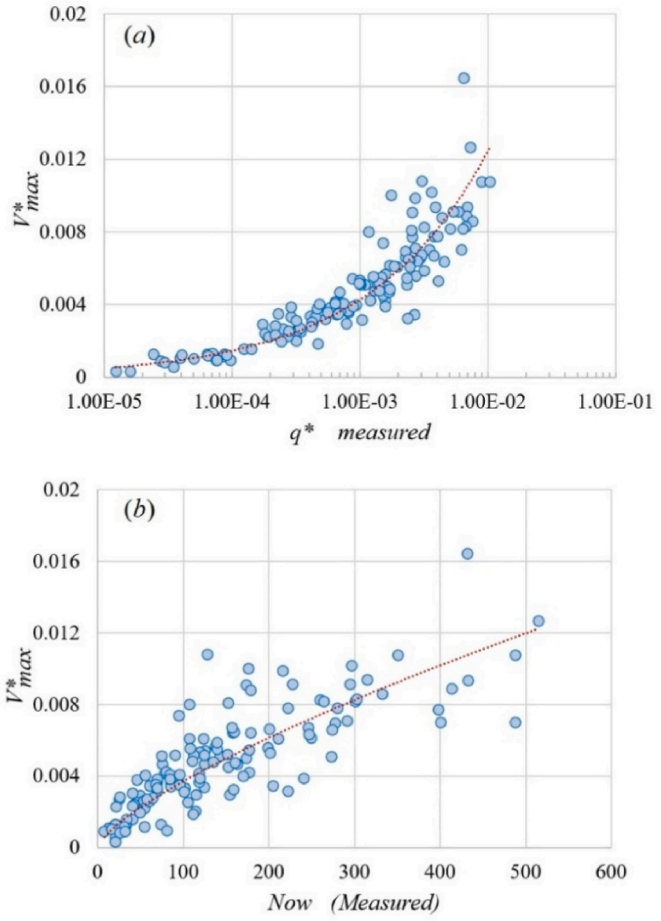


**Fig. 10.** (a) Relationship between the measured dimensionless mean overtopping rate ($q^*$) and $V^*_{max}$. (b) Relationship between the measured number of overtopping waves ($N_{ow}$) and $V^*_{max}$.

distributions (Models W1 and E1), respectively. Moreover, the estimation of $V^*_{max}$ using Eq. (38) reduced the *NBIAS* and *SI* values by 46% and 38% in comparison to the most accurate existing one when the estimators of $N_{ow}$ and $q^*$ were used. The corresponding scatter plot for different formulations, using estimated $N_{ow}$ and $q^*$ are shown in Fig. 11. As seen, the underestimation of $V^*_{max}$ using Molines et al. (2019) is significant, although this is the best performing existing expression. Models W1 and E1 are the most accurate formulae of Weibull and Exponential distributions obtained from the weighted fitting (derived in sections 5.3 and 5.4 respectively).

Eq. (38) with almost zero bias (*NBIAS* = −6) represents the best fit. However, for practical design purposes, a safety margin with an acceptable level of risk needs to be considered. This can be achieved by assuming that the coefficients of the formula are stochastic variables with a normal distribution (EurOtop, 2018). In this study, following

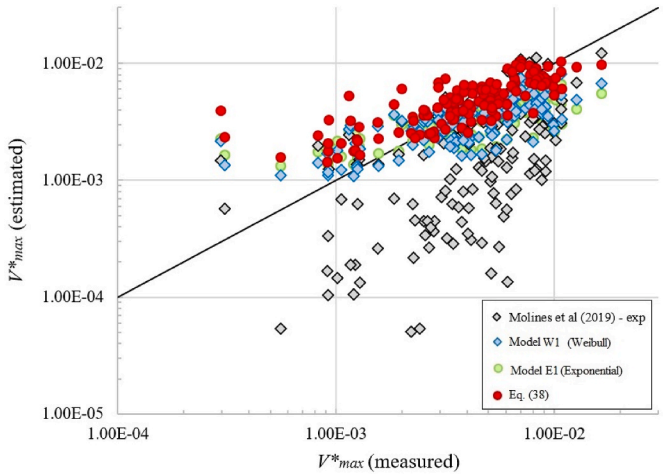


**Fig. 11.** Measured vs estimated $V^*_{max}$ using Molines et al. (2019), as the best existing formula, Models W1 and E1 (bests of the Weibull and Exponential distributions) and Eq. (38).

TAW (2002), one standard deviation of the coefficient $\sigma$ (0.0125) = $1.84\times 10^{-3}$ was added to obtain the design formula as below:

$$V^*_{max} = 0.0143\ N_{ow}^{0.23}.q^{*0.28} \tag{39}$$

### 5.6. Study scope and recommendations for future studies

The scope of the present study and the developed formulae for the estimation of individual wave overtopping volumes and $V_{max}$ is limited to rubble mound seawalls with an impermeable core within the given range of test parameters. Hence, verification or modification of the proposed formulations for different conditions such as shallow water ($h/H_{m0}$), milder slopes ($cot\ \alpha > 2$) or seawalls with a crown wall are recommended for future studies. It is also recommended to verify if a relatively simple empirical expression to estimate maximum overtopping volumes can outperform more complicated expressions based on Weibull or Exponential expressions for other types of coastal structures.

Another issue to be pointed out is the uncertainty that arises from the variability of wave overtopping parameters. Few studies (e. g. Romano et al., 2015; Vieira et al., 2021; Williams et al., 2019) have been devoted to investigate the variability of the mean wave overtopping measurement ($q$) using different time series as input. Romano et al. (2015) conducted several tests on breakwaters and stated that the variability of $q$ may reach one order of magnitude when different time series realisations from the same wave spectrum are used. It is likely that various realisations from the same wave spectrum can affect the volumes per overtopping wave, especially for the maximum volume $V_{max}$.

## 6. Conclusions

To determine the crest elevation of rubble mound seawalls, the accurate estimation of the maximum individual overtopping volume ($V_{max}$ or $V_{0.1\%}$) is an important factor. This research aimed to better understand the distribution of individual overtopping volumes at rubble mound seawalls with an impermeable core and to improve the existing predictive tools for the estimation of $V_{max}$. For this purpose, 2D small-scale physical model tests were conducted on a 2-layer rubble mound seawall with the seaward slopes of 1:1.5 and 1:2 covering $0.75 \leq R_c/H_{m0} \leq 2.5$.

The estimation of $V_{max}$ using distribution-based methods depends on parameters such as the number of overtopping waves ($N_{ow}$) and mean overtopping discharge ($q$). As expected, using measured $q$ and $N_{ow}$ lead to a more accurate estimation of the $V_{max}$ compared to using the estimated values of mentioned parameters. However, as $q$ and $N_{ow}$ are not available in practice, the analysis of the results should focus on the estimation of $V_{max}$ using the estimated $q$ and $N_{ow}$.

To evaluate the ability of the existing formulae to estimate $V_{max}$, the original estimators of $q$ and $N_{ow}$ (proposed by their authors), were used. For the formulae developed in this study, the best estimators of $N_{ow}$ (Eqs. (22), (23) and (25)) and $q$ (Eq. (35)) at rubble mound seawalls with an impermeable core were used. All existing formulae (based on either the Weibull or Exponential distributions), underestimate the non-dimensional $V^*_{max}$ ($= \frac{V_{max}}{gHm0T_m^2}$). The formula of Molines et al. (2019) provided the most accurate estimation with $NIBAS = -52\%$ and $SI = 75\%$. The underestimation of $V^*_{max}$ given by the Molines et al. (2019) formula is because it has been derived for conventional mound breakwaters with a permeable core. Hence, less overtopping is expected compared to seawalls with an impermeable core as per the present dataset.

The 2-parameter Weibull distribution was fitted to the data using 10%, 30%, and 50% of the highest overtopping volumes as well as using the weighted method proposed by Molines et al. (2019). The Weibull shape factor ($b$) was related to $q^*$ using an exponential function. Then, a linear regression fit was proposed to estimate the Weibull scale factor ($a$). Similar to the results reported by Mares-Nasarre et al. (2020) and Molines et al. (2019), the weighted method (Model W1), with $NBIAS = -21$ and $SI = 52\%$, provided a more accurate estimation of $V^*_{max}$ in comparison to the other formulae.

The 2-parameter Exponential distribution was used to estimate $V^*_{max}$ using the same scenarios (i.e. sampling the data using 10%, 30%, and 50% of the highest overtopping volumes and using the weighted method). A power function of $q^*$ was proposed to estimate parameter $D$, while parameter $C$ was estimated using a linear function of $D$. The weighted method (Model E1), with $NBIAS = -31\%$ and $SI = 58\%$, performed better than the models in which the lower values of the overtopping volumes are removed. A comparison of the best models showed that Model W1 (Weibull) is slightly more accurate than Model E1 (Exponential). The re-calibrated Model W1 also showed an improvement of 23% in $SI$ value in comparison to the best of the existing ones.

A new simple empirical formula (Eq. (38)) was proposed as an alternative to the distribution-based approaches. This formula correlates $V^*_{max}$ to $N_{ow}$ and $q^*$ through a power function and is physically justifiable as $V^*_{max} = 0$ for either $N_{ow} = 0$ or $q^* = 0$. The results of estimation of $V^*_{max}$ using Eq. (38) demonstrated its superiority to the distribution-based methods including those developed within the present study as well as proposed in the literature. With $NBIAS = -6\%$ and $SI = 37\%$, Eq. (38) demonstrated a better bias as well as improvements of 21%, 15%, and 38% in $SI$ values compared to the Model E1 (best of Exponential distribution), Model W1 (best of Weibull distribution) and Molines et al. (2019) formula (best of existing ones), respectively.

## CRediT authorship contribution statement

**Ali Koosheh:** Conceptualization, Methodology, Formal analysis, Investigation, Data curation, Writing – original draft, Visualization. **Amir Etemad-Shahidi:** Conceptualization, Methodology, Formal analysis, Supervision, Writing – review & editing. **Nick Cartwright:** Conceptualization, Supervision, Writing – review & editing. **Rodger Tomlinson:** Conceptualization, Supervision, Writing – review & editing. **Marcel R.A. van Gent:** Conceptualization, Supervision, Writing – review & editing.

## Declaration of competing interest

The authors declare that they have no known competing financial interests or personal relationships that could have appeared to influence the work reported in this paper.

## Acknowledgments

The authors would like to acknowledge the financial support from Griffith University. The first author was funded by GUPRS and GUIPRS scholarships. Patricia Mares-Nasarre is also acknowledged for her advice on instrumentation and experimental set up.

## Appendix A

EurOtop (2018) formula to estimate mean overtopping rate at rubble mound structures

$$\frac{q}{\sqrt{g \cdot H_{m0}^3}} = 0.09 \cdot \exp\left[-\left(1.5 \frac{R_c}{H_{m0} \cdot \gamma_f \cdot \gamma_\beta}\right)^{1.3}\right]$$

## Appendix B

**Table A1**
Details of estimation of $V_{max}$ using the existing formulae based on their original estimators of $N_{ow}$ and $q$.

| Formula | Parameters of distribution | $N_{ow}$ estimator | $q$ estimator |
|---|---|---|---|
| van der Meer and Janssen (1994) | $b = 0.75$ $a$: Eq. (3) | Eqs. 22–24 | $Ir_p < 2\ \frac{q}{\sqrt{gH_{m0}^3}}\sqrt{\frac{s_{op}}{\tan\alpha}} = 0.06\ exp\left(-5.2\frac{R_c}{H_{m0}}\frac{\sqrt{s_{op}}}{\tan\alpha}\frac{1}{\gamma_f\gamma_h\gamma_\beta}\right)$ $Ir_p > 2;\ \frac{q}{\sqrt{gH_{m0}^3}} = 0.2\ exp\left(-2.6\frac{R_c}{H_{m0}}\frac{1}{\gamma_f\gamma_h\gamma_\beta}\right)$ |
| Zanuttigh et al. (2013), * | $b$: Eq. (8) $a$: Eq. (3) | Eqs. (22), (23) and (25) | $\frac{q}{\sqrt{g\,.\,H_{m0}^3}} = 0.09.\ \exp\left[-\left(1.5\frac{R_c}{H_{m0}\cdot\gamma_f\cdot\gamma_\beta}\right)^{1.3}\right]$ |
| Molines et al. (2019) | $b$: Eq. (10) $A$: Eq. (11) | Eq. (27) | CLASH – NN |
| Molines et al. (2019) | $D$: Eq. (17) $C$: Eq. (18) | Eq. (27) | CLASH – NN |
| Mares-Nasarre et al. (2020) | $b$: Eq. (19) $A$: Eq. (20) | Eq. (28) | CLASH - NN |

* Suggested by EurOtop (2018).

## Appendix C

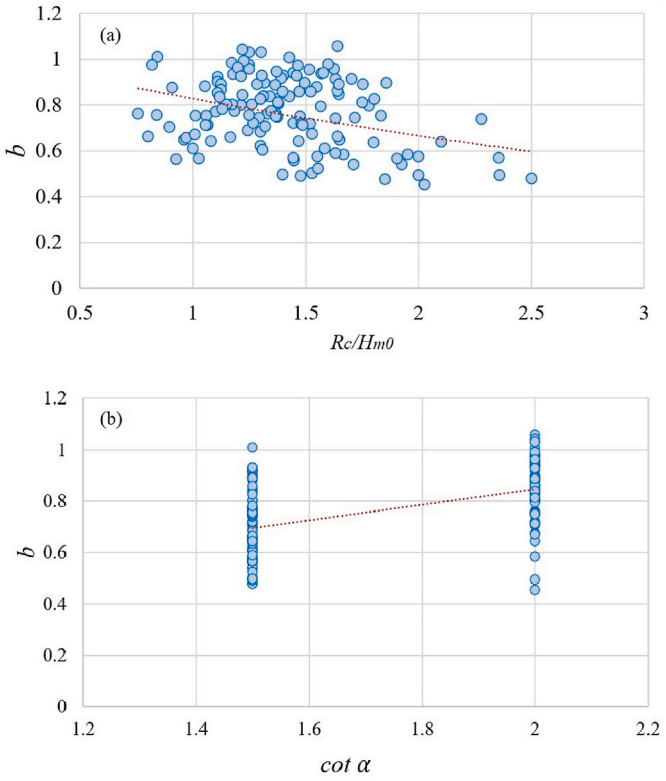


**Fig. A1.** Weibull shape factor against (a): relative crest freeboard, (b): seaward slope (Weighted method)

**Table A2**
The accuracy metrics of Weibull fit (weighted method) based on wave and structural parameters

| b | a | *NBIAS* (%) | *SI* (%) |
|---|---|---|---|
| $exp\ (0.24\ \frac{R_c}{H_{m0}}) + 0.29\ \cot\alpha - 0.57$ | Eq. (3) | −49 | 68 |

## Appendix D

**Table A3**
The accuracy metrics of formulae developed for smooth sloped structures to estimate $V^*_{max}$

| Author | Weibull shape factor ($b$) | *NBIAS* (%) | *SI* (%) |
|---|---|---|---|
| Victor et al. (2012) | $b = exp\ (-2.0\ \frac{R_c}{H_{m0}}) + 0.15\ \cot\alpha + 0.56$ | −77 | 89 |
| Hughes et al. (2012) | $b = \left[exp\left(-0.6\frac{R_c}{H_{m0}}\right)\right]^{1.8} + 0.64$ | −75 | 79 |
| Gallach-Sánchez (2018) | $b = (0.59 + 0.23\ \cot\alpha)\ exp\ (-2.2\ \frac{R_c}{H_{m0}}) + 0.83$ | −71 | 87 |

As seen, they led to the less accurate estimation of $V_{max}$ compared to formulae proposed for rough structures.

## Appendix E

As an example, the maximum individual overtopping volume ($V_{max}$) is estimated for a real rubble mound seawall. The design conditions are: $H_{m0} = 3.0$ m, $T_p = 11.1$ s $T_m = 9.7$ s, $T_{m\text{-}1,0} = 10.1$ s, $h = 9.9$ m, rock two-layer, impermeable core, $\gamma_f = 0.55$, $\cot\alpha = 1.75$, $R_c = 5.08$ m.
Estimation of $N_{ow}$ using EurOtop (2018) formula:
$L_{m\text{-}1,0} = g/2\pi\ T^2_{m\text{-}1,0} = 1.56 \times 10.1^2 = 159.3$ m
$s_{m\text{-}1,0} = H_{m0}/L_{m\text{-}1,0} = 3.0/159.3 = 0.0188$.
$Ir_{m\text{-}1,0} = \tan\alpha/\sqrt{s_{m\text{-}1,0}} = 0.57/\sqrt{0.0188} = 4.15$

$$\gamma_{f\_surging} = \gamma_f + \frac{(Ir_{m-1,0} - 1.8)(1 - \gamma_f)}{8.2} = 0.55 + \frac{(4.15 - 1.8)(1 - 0.55)}{8.2} = 0.68$$

$$\frac{R_{u2\%}}{H_{m0}} = = \min\left(1.65\ \gamma_f\gamma_\beta Ir_{m-1,0},\ 1.0\ \gamma_{f\_surging}\gamma_\beta\left(4 - \frac{1.5}{\sqrt{Ir_{m-1,0}}}, 3\right)\right) = 2.21$$

$$\chi = \frac{1}{\sqrt{-ln(0.02)}} \cdot \frac{R_{u2\%}}{H_{m0}} = 1.12$$

$$P_{ow} = \exp\left(-\left(\frac{1}{\chi}\frac{R_c}{H_{m0}}\right)^2\right) = 0.10$$

Assuming 6 h for storm duration.
$N_{ow} = P_{ow}.\ N_w = 0.10 \times 2230 = 223$.
Estimation of $q$ using Koosheh et al. (2022) formula:
$q^* = \frac{q}{\sqrt{gH^3_{m0}}} = 0.034\ exp\ [-4.97\ \left(\frac{R_c}{H_{m0}\cdot\gamma_f}\right)^{1.12}(s_{m-1,0})^{0.35}] = 0.00043$
$q = 0.007$ m$^3$/s/m.
Model W1:
$b = 0.722\ exp\ (22.41q^*) = 0.729$.
$A = 1.8 - \frac{0.35}{b} = 1.32$
$a = \frac{A\ qT_m}{P_{ow}} = 0.896$.
$V_{max} = a\ [ln(N_{ow} + 1)]^{1/b} = 9093$ l/m.
Model E1:
$D = 0.710\ q^{*-0.190} = 3.05$.
$C = 2.7\text{–}1.96D = -3.10$

$$\overline{V} = \frac{qT_mN_w}{N_{ow}} = 0.68$$

$V_{max} = D\ \overline{V}\ [ln(N_{ow} + 1) + C/D] = 9120$.
Eq. (38)

$$V^*_{max} = 0.0125\ N_{ow}^{0.23} \cdot q^{*0.28} = 0.00495$$

$V_{max} = g\ H_{m0}\ T_m^2 V^*_{max} = 13680$ l/m.

**Table A4**
Estimation of $V_{max}$ using existing formulae and proposed ones

| Formula | $V_{max}$ (l/m) |
|---|---|
| van der Meer and Janssen (1994) | 1276 |
| Zanuttigh et al. (2013) | 4440 |
| Molines et al. (2019) - Weibull | 7415 |
| Molines et al. (2019) - Exponential | 7204 |
| Mares-Nasarre et al. (2020) | 7835 |
| Model W1 | 9093 |
| Model E1 | 9120 |
| Eq. (38) | 13680 |

## Appendix F

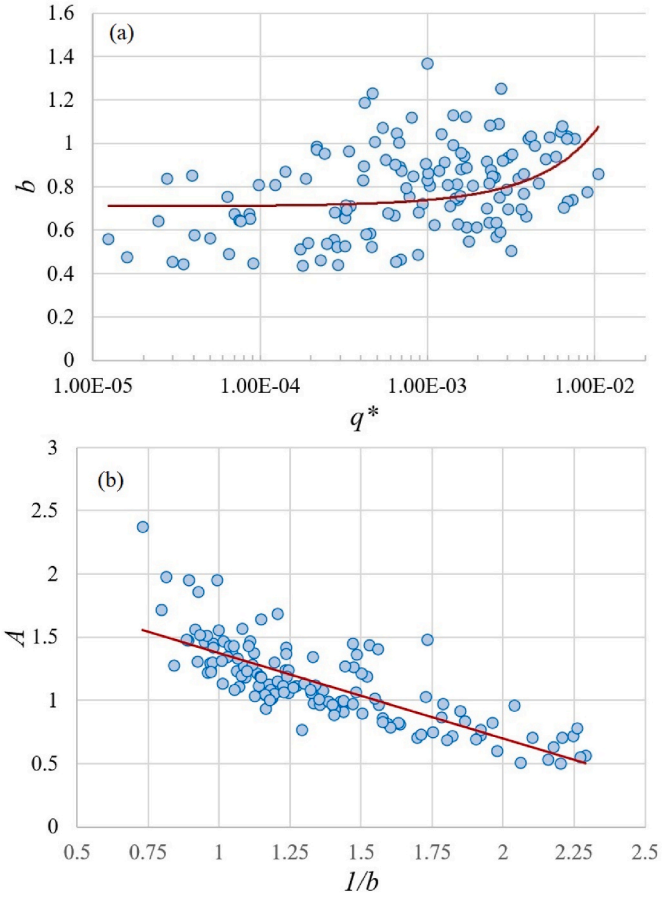


**Fig. A2.** (a): Relationship between measured dimensionless mean overtopping rate ($q^*$) and Weibull shape factor; (b): relationship between $1/b$ and A using 50% upper volumes

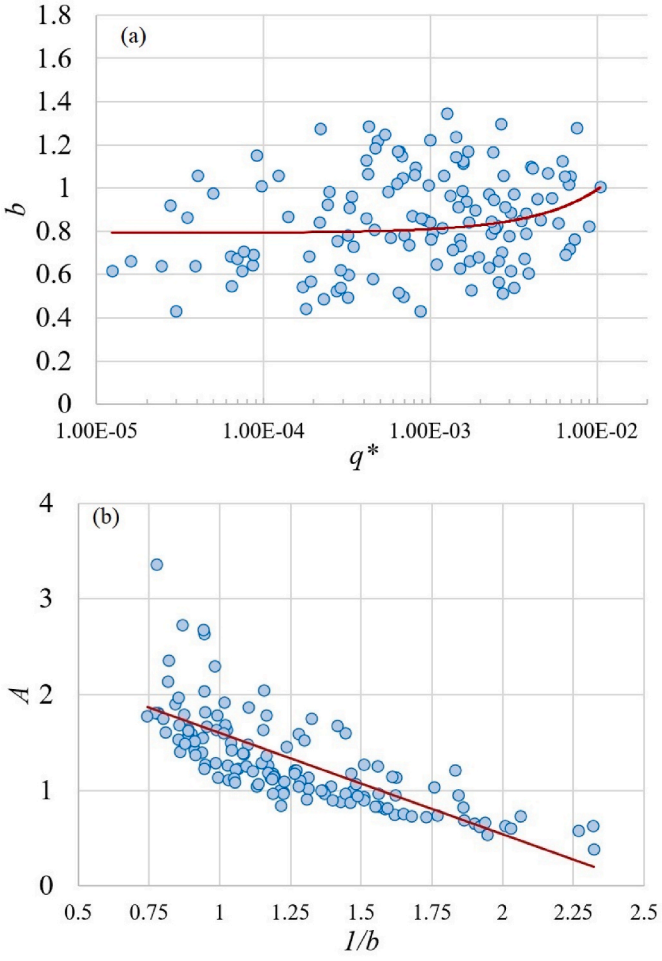


**Fig. A3.** (a): Relationship between measured dimensionless mean overtopping rate ($q^*$) and Weibull shape factor; (b): relationship between $1/b$ and A using 30% upper volumes

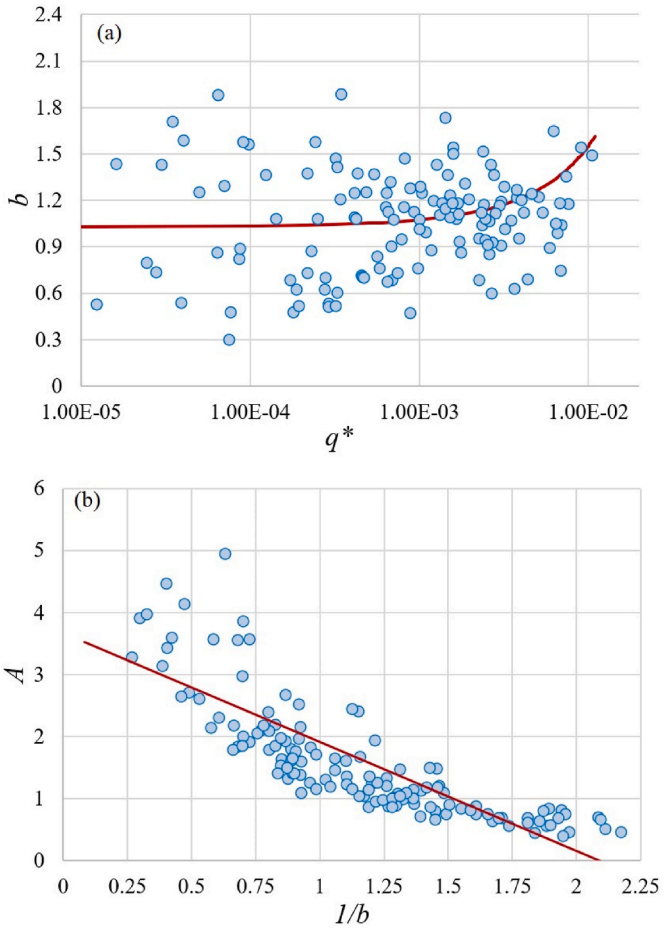


**Fig. A4.** (a): Relationship between measured dimensionless mean overtopping rate ($q^*$) and Weibull shape factor; (b): relationship between $1/b$ and A using 10% upper volumes

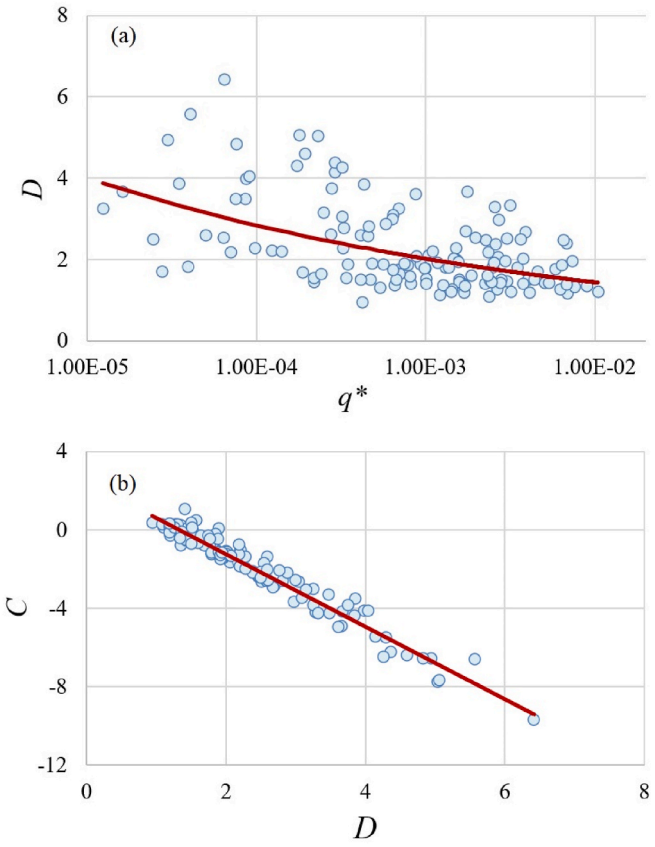


**Fig. A5.** (a) Relationship between the measured dimensionless mean overtopping rate ($q^*$) and $D$; (b) relationship between $D$ and $C$ using the 50% upper volumes (Exponential distribution)

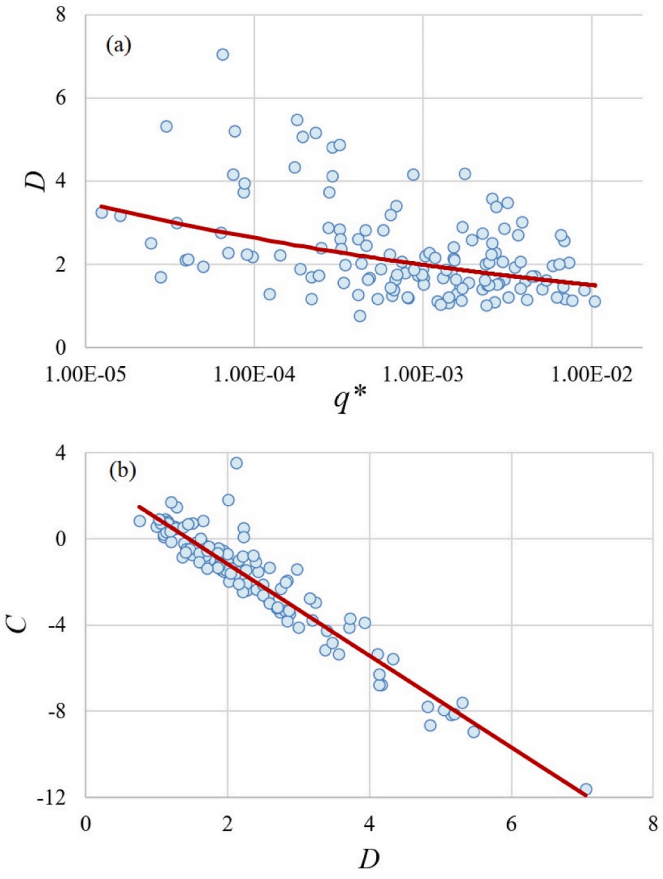


**Fig. A6.** (a) Relationship between the measured dimensionless mean overtopping rate ($q^*$) and $D$; (b) relationship between $D$ and $C$ using the 30% upper volumes (Exponential distribution)

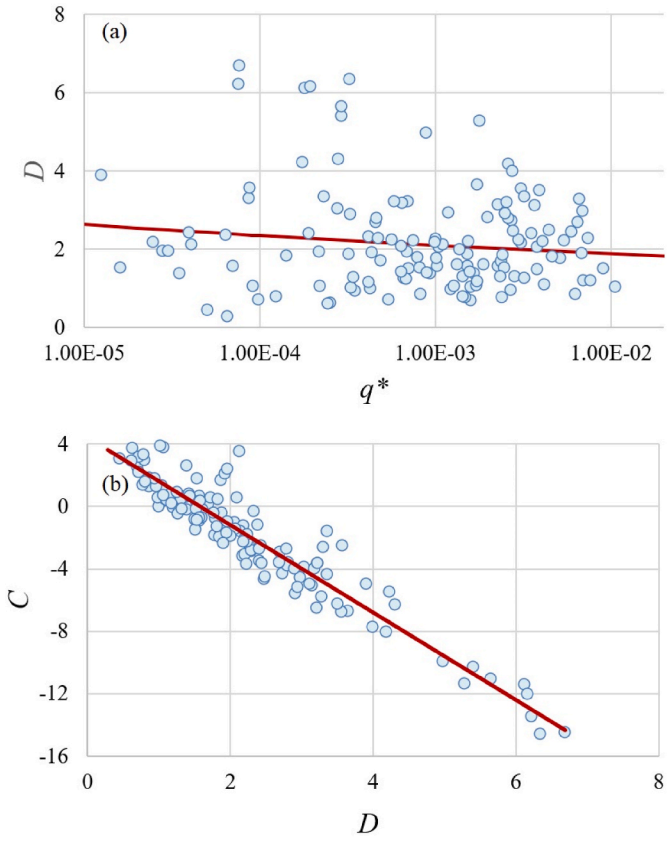


**Fig. A7.** (a) Relationship between the measured dimensionless mean overtopping rate ($q^*$) and $D$; (b) relationship between $D$ and $C$ using the 10% upper volumes (Exponential distribution)

## Appendix G

**Table A5**

Accuracy metrics of formulae in the literature for the estimation of $V^*_{max}$ ($=\frac{V_{max}}{gHm0T_m^2}$) using the best estimators of $N_{ow}$ and $q$

| Formula | Estimated $q$ and $N_{ow}$ | |
|---|---|---|
| | *NBIAS* (%) | *SI* (%) |
| van der Meer and Janssen (1994) | −56 | 73 |
| Zanuttigh et al. (2013)* | −64 | 81 |
| Molines et al. (2019) - Weibull | −39 | 60 |
| Molines et al. (2019) - Exponential | −37 | 60 |
| Mares-Nasarre et al. (2020) | −54 | 73 |

## References


Besley, P., 1999. Wave Overtopping of Seawalls, Design and Assessment Manual. R&D technical report W178D, HR Wallingford.

Bruce, T., van der Meer, J.W., Franco, L., Pearson, J.M., 2009. Overtopping performance of different armour units for rubble mound breakwaters. Coast. Eng. 56, 166–179.

Ciria, C., 2007. CETMEF (2007). The Rock Manual. The Use of Rock in Hydraulic Engineering. Publicação.

Etemad-Shahidi, A., Bali, M., van Gent, M.R.A., 2020. On the stability of rock armored rubble mound structures. Coast. Eng. 158, 103655.

EurOtop, 2007. In: Pullen, T., Bruce, T., van der Meer, N.L.J.W., Schüttrumpf, H., Kortenhaus, A. (Eds.), Wave Overtopping of Sea Defences and Related Structures–Assessment Manual. NWH Allsop. www.overtopping-manual.com.

EurOtop, 2018. In: van der Meer, J.W., Allsop, N.W.H., Bruce, T., De Rouck, J., Kortenhaus, A., Pullen, T., Schüttrumpf, H., Troch, P., Zanuttigh, B. (Eds.), Manual on Wave Overtopping of Sea Defences and Related Structures. www.overtopping-manual.com.

Formentin, S.M., Zanuttigh, B., 2019. Semi-automatic detection of the overtopping waves and reconstruction of the overtopping flow characteristics at coastal structures. Coast. Eng. 152, 103533 https://doi.org/10.1016/j.coastaleng.2019.103533.

Franco, L., de Gerloni, M., van der Meer, J.W., 1995. Wave overtopping on vertical and composite breakwaters. In: Proc. 24th International Conference on Coastal Engineering, pp. 1030–1044. https://doi.org/10.1061/9780784400890.076.

Gallach-Sánchez, D., 2018. Experimental Study of Wave Overtopping Performance of Steep Low-Crested Structures. PhD Thesis. Ghent University.

Hughes, S.A., Thornton, C.I., van der Meer, J., Scholl, B., 2012. Improvements in describing wave overtopping processes. Proc. Coast. Eng. Conf. 1–15. https://doi.org/10.9753/icce.v33.waves.35.

Hughes, S.A., Thornton, C.I., 2016. Estimation of time-varying discharge and cumulative volume in individual overtopping waves. Coast. Eng. 117, 191–204. https://doi.org/10.1016/j.coastaleng.2016.08.006.

Jafari, E., Etemad-Shahidi, A., 2011. Derivation of a new model for prediction of wave overtopping at rubble mound structures. J. Waterw. Port, Coast. Ocean Eng. 138, 42–52. https://doi.org/10.1061/(ASCE)WW.1943-5460.0000099.

Ju, Q., Liu, S., Huang, W., Zhong, G., 2019. Berm effects on the probability distribution of individual wave overtopping discharge over a low-crested sea Dike. J. Waterw. Port, Coast. Ocean Eng. 145, 04019012 https://doi.org/10.1061/(asce)ww.1943-5460.0000507.

Koosheh, A., Etemad-Shahidi, A., Cartwright, N., Tomlinson, R., Hosseinzadeh, S., 2020. The comparison of empirical formulae for the prediction of mean wave overtopping rate at armored sloped structures. Coast. Eng. Proc. 22.
Koosheh, A., Etemad-Shahidi, A., Cartwright, N., Tomlinson, R., van Gent, M.R.A., 2022. Experimental study of wave overtopping at rubble mound seawalls. Coast. Eng. 172, 104062.
Koosheh, A., Etemad-Shahidi, A., Cartwright, N., Tomlinson, R., van Gent, M.R.A., 2021. Individual wave overtopping at coastal structures: a critical review and the existing challenges. Appl. Ocean Res. 106, 102476.
Lykke Andersen, T., Burcharth, H.F., Gironella, F.X., 2009. Single wave overtopping volumes and their travel distance for rubble mound breakwaters. Coast.Struct. 1241–1252. https://doi.org/10.1142/9789814282024_0109.
Mansard, E.P.D., Funke, E.R., 1980. The measurement of incident and reflected spectra using a least squares method. In: Coastal Engineering 1980, pp. 154–172.
Mares-Nasarre, P., Molines, J., Gómez-Martin, M.E., Medina, J.R., 2020. Individual wave overtopping volumes on mound breakwaters in breaking wave conditions and gentle sea bottoms. Coast. Eng., 103703
Molines, J., Herrera, M.P., Gómez-Martín, M.E., Medina, J.R., 2019. Distribution of individual wave overtopping volumes on mound breakwaters. Coast. Eng. 149, 15–27. https://doi.org/10.1016/j.coastaleng.2019.03.006.
Nørgaard, J.Q.H., Andersen, T.L., Burcharth, H.F., Steendam, G.J., 2013. Analysis of overtopping flow on sea dikes in oblique and short-crested waves. Coast. Eng. 76, 43–54.
Owen, M.W., 1980. Design of Seawalls Allowing for Wave Overtopping (Report No. Ex 924). Hydraul. Res. HR Wallingford.
Pan, Y., Li, L., Amini, F., Kuang, C., Chen, Y., 2016. New understanding on the distribution of individual wave overtopping volumes over a levee under negative freeboard. J. Coast Res. 75, 1207–1211. https://doi.org/10.2112/si75-242.1.
Romano, A., Bellotti, G., Briganti, R., Franco, L., 2015. Uncertainties in the physical modelling of the wave overtopping over a rubble mound breakwater: the role of the seeding number and of the test duration. Coast. Eng. 103, 15–21.
Schüttrumpf, H., van Gent, M.R.A., 2003. Wave overtopping at seadikes. In: Coast. Struct. 2003 - Proc. Conf., 40733, pp. 431–443. https://doi.org/10.1061/40733(147)36.
Shaeri, S., Etemad-Shahidi, A., 2021. Wave overtopping at vertical and battered smooth impermeable structures. Coast. Eng. 166, 103889.
Smolka, E., Zarranz, G., Medina, J.R., 2009. Estudio experimental del rebase de un dique en talud de cubpodos. In: Libro de Las X Journadas Espanolas de Costas y Puertos. Universidad de Cantabria-Adif Congresos, pp. 803–809.
Su, J.C., Liu, C.I., Kuo, C.T., 1992. Application of Weibull distribution for irregular wave overtopping. In: Proc. Of 6th IAHR Symp. on Stochastic Hyd., Taipei, Taiwan.
TAW, 2002. Technical Report Wave Run-up and Wave Overtopping at Dikes. Tech. Advis. Comm. Flood Defence. Delft, Netherlands.
US Army Corps of Engineers, 2002. Coastal engineering manual. Eng. Manag. 1110–2-1100.
van der Meer, J., Bruce, T., 2014. New physical insights and design formulas on wave overtopping at sloping and vertical structures. J. Waterw. Port, Coast. Ocean Eng. 140, 1–18. https://doi.org/10.1061/(ASCE)WW.1943-5460.0000221.
van der Meer, J.W., Janssen, J., 1994. Wave Run-Up and Wave Overtopping at Dikes and Revetments. VdM VML EB MT2. Delft Hydraulics, publication no. 485.
van Gent, M.R.A., 2002. Low-exceedance Wave Overtopping Events: Measurements of Velocities and the Thickness of Water-Layers on the Crest and Inner Slope of Dikes. Delft Cluster, Dc030202/H3803.
van Gent, M.R.A., van den Boogaard, H.F.P., Pozueta, B., Medina, J.R., 2007. Neural network modelling of wave overtopping at coastal structures. Coast. Eng. 54, 586–593.
Victor, L., van der Meer, J.W., Troch, P., 2012. Probability distribution of individual wave overtopping volumes for smooth impermeable steep slopes with low crest freeboards. Coast. Eng. 64, 87–101. https://doi.org/10.1016/j.coastaleng.2012.01.003.
Vieira, F., Taveira-Pinto, F., Rosa-Santos, P., 2021. New developments in assessment of wave overtopping on single-layer cube armoured breakwaters based on laboratory experiments. Coast. Eng. 166, 103883.
Williams, H.E., Briganti, R., Romano, A., Dodd, N., 2019. Experimental analysis of wave overtopping: a new small scale laboratory dataset for the assessment of uncertainty for smooth sloped and vertical coastal structures. J. Mar. Sci. Eng. 7, 217. https://doi.org/10.3390/jmse7070217.
Zanuttigh, B., van der Meer, J., Bruce, T., Hughes, S., 2013. Statistical characterisation of extreme overtopping wave volumes. Coasts, Mar. Struct. Break. 2013 from Sea to Shore - Meet. Challenges Sea. https://doi.org/10.1680/fsts.59757.0442, 1, 442-451.

## Glossary

$a$: Weibull scale factor
$b$: Weibull shape factor
$c$: Adjusting parameter of the Exponential distribution
$c_s$: Minimum possible celerity
$c_d$: Maximum wave celerity defined by $L_{0p}/T_p$
$d$: Adjusting parameter of the Exponential distribution
$d_w$: Distance between two wave gauges in the direction of the overtopping
$C$: Dimensionless parameter of the Exponential distribution defined by $c/\overline{V}$
$D$: Dimensionless parameter of the Exponential distribution defined by $d/\overline{V}$
$D_{n50}$: Nominal Median rock size
$g$: Gravity acceleration
$G_c$: Crest width
$h$: Water depth at the structure's toe
$h_c$: Overtopping flow thickness
$H_{m0}$: Spectral significant wave height
$H_{1/10}$: Average of 1/10 highest incident waves
$Ir_p$: Iribarren number defined by $tan\ \alpha/\sqrt{s_{op}}$
$Ir_{m-1,0}$: Iribarren number defined by $tan\ \alpha/\sqrt{s_{m-1,0}}$
$L_{op}$: Wavelength defined by $gT_p^2/2\pi$
$N_{ow}$: Number of overtopping waves
$N_w$: Number of incident waves
$S_f$: Sampling rate
$P_{ow}$: Probability of overtopping
$P_v$: Exceedance probability of an individual overtopping volume
$q$: Mean overtopping discharge per metre of structure width
$q^*$: Dimensionless mean overtopping discharge defined by $q/\sqrt{gH_{m0}^3}$
$Q^*$: Dimensionless mean overtopping discharge defined by $q/gT_mH_{m0}$
$r_s$: Threshold value for time-domain-down-crossing algorithm
$R_c$: Crest freeboard
$R_{u2\%}$: Run-up height exceeded by 2% of incident waves
$s_{op}$: Wave steepness defined by $2\pi H_{m0}/gT_p{}^2$
$s_{om}$: Wave steepness defined by $2\pi H_{m0}/gT_m{}^2$
$s_{m-1,0}$: Wave steepness defined by $2\pi H_{m0}/gT_{m-1,0}{}^2$
$T_m$: Mean wave period
$T_{m-1,0}$: Spectral wave period
$T_p$: Peak wave period
$V_c$: Cumulative overtopping volume
$V_{max}$: Maximum individual overtopping volume
$V^*_{max}$: Dimensionless maximum individual overtopping volume ($V_{max}/g\ H_{m0}\ T_m^2$)
$\overline{V}$: Mean individual overtopping volume
$V_i$: Individual overtopping volume
$V_{0.1\%}$: Individual overtopping volume exceeded by less than 0.1% of the incident waves
$w_i$: Assigned weight for an individual overtopping volume
$\alpha$: Seaward slope of structure
$\Gamma$: Gamma function
$\gamma_\beta$: Oblique wave factor
$\gamma_f$: Roughness factor
$\gamma_{fmod}$: Modified roughness factor
$\gamma_h$: Water depth factor